REPORT DOCUMENTATION PAGE

AFRL-SR-AR-TR-05-

0377

1. REPORT DATE (DD-MM-YYYY)	2. REPORT TYPE	3. DATES COVERED (From - To)
14-02-2005	Final	01-01-2004 to 31-12-2004

4. TITLE AND SUBTITLE

Improved Single Photon Detectors for Telecom Wavelengths

Year Three (Final) Report

5a. CONTRACT NUMBER

F49620-01-1-0551

5b. GRANT NUMBER

5c. PROGRAM ELEMENT NUMBER

6. AUTHOR(S)

William P. Risk

5d. PROJECT NUMBER

5e. TASK NUMBER

5f. WORK UNIT NUMBER

7. PERFORMING ORGANIZATION NAME(S) AND ADDRESS(ES)

IBM Research Division
IBM Almaden Research Center
650 Harry Road
San Jose, CA 95120

8. PERFORMING ORGANIZATION REPORT NUMBER

DARPA Quist FINAL

9. SPONSORING/MONITORING AGENCY NAME(S) AND ADDRESS(ES)

USAF, ARFL
AF Office of Scientific Research
4015 Wilson Blvd Room 713
Arlington, VA 22203-1954

NE

10. SPONSOR/MONITOR'S ACRONYM(S)

DARPA/AFOSR

11. SPONSOR/MONITOR'S REPORT NUMBER(S)

12. DISTRIBUTION/AVAILABILITY STATEMENT

Approved for public release, distribution unlimited

13. SUPPLEMENTARY NOTES

14. ABSTRACT

In this final report for the DARPA QuIST program entitled "Single Photon Detectors For Telecom Wavelengths," we describe progress made in Year Three of the program. We describe continued progress by UT Austin and UCSD in developing novel semiconductor detectors that perform well as single photon counters and in understanding the sources of dark counts that limit the single-photon-counting performance of these devices. We also report on IBM's production and distribution to QuIST partners of research prototype single photon detectors based on commercially-available InGaAs APDs coupled with specialized electronic circuitry developed at IBM. Finally, we report progress toward using nonlinear sum-frequency generation as an alternative to InGaAs detectors.

15. SUBJECT TERMS

16. SECURITY CLASSIFICATION OF:			17. LIMITATION OF ABSTRACT	18. NUMBER OF PAGES	19a. NAME OF RESPONSIBLE PERSON
a. REPORT	b. ABSTRACT	c. THIS PAGE			William P. Risk
UU	UU	UU	UU	35	19b. TELEPHONE NUMBER (Include area code) (408) 927-2467

Improved Single Photon Detectors for Telecom Wavelengths

Year Three (Final) Progress Report

Contract #F49620-01-1-0551 (DARPA QuIST Program)

Principal Investigator:
William P. Risk
IBM Almaden Research Center
650 Harry Rd., MS K13/D2
San Jose, CA 95120
risk@almaden.ibm.com
Ph. 408-927-2467
Fax 408-927-2100

I. Introduction

A. Background

The development of practical quantum key distribution (QKD) systems depends upon the availability of efficient, low-noise single-photon detectors. An important class of QKD systems is designed to use standard telecommunications optical fiber as the link conveying quantum information, and therefore operation at a wavelength of 1310 or 1550 nm is required. In order to detect single photons at these wavelengths, commercially-available Ge or InGaAs avalanche photodiodes (APDs) have been used, albeit in a manner for which they were not designed—generally, they must be cooled to low temperatures (~77–150K) and operated above their reverse breakdown voltages ("Geiger mode") in order to detect single photons with acceptably high detection efficiencies and acceptably low dark count rates.

Under the extreme operating conditions required for single-photon detection, there is a wide variability in the performance of detectors from manufacturer-to-manufacturer, and even from device-to-device made by the same manufacturer. Moreover, as manufacturers have refined successive generations of APDs in order to improve their performance in standard telecom applications, they have actually made them worse for single-photon detection.

A further very severe problem is that specific APDs that have been used in past QKD experiments are now becoming unavailable to researchers. In some cases, large-volume orders by optical network developers are consuming the entire supply of some devices; others are no longer available as discrete detectors, but are being packaged with other components (e.g., GaAs preamplifiers) in a way that makes them unsuitable for use as single-photon counters; still others are being discontinued as demand declines due to the slowdown in the telecom industry.

Hence, in order to continue the advancement of QKD systems and to enable new experiments involving transport of quantum information over long distances via optical fiber, it is essential to develop new detectors with high detection efficiency and low dark count rate.

B. Program Objectives:

1. To understand, through modeling and experimentation, the physical parameters that are most important for achieving high-efficiency, low-noise detection of single 1310/1550 nm photons using avalanche photodiodes.
2. Using this understanding, to design, fabricate, and characterize APDs for single-photon detection at telecom wavelengths
3. To test these improved APDs in a quantum cryptography system and understand how the improved detector characteristics improve the performance of the QKD system.
4. To investigate nonlinear frequency conversion combined with Si APDs as an alternative to the use of InGaAs APDs for detection of single telecom-wavelength photons.

C. Program Participants:

IBM Research
Almaden Research Center
Dr. William P. Risk (PI)
Dr. Donald S. Bethune

University of Texas at Austin
Prof. Joe C. Campbell & graduate students

University of California at San Diego
Prof. Yu-Hwa Lo & graduate students

D. Program Approaches:

Under this program, we are pursuing three independent approaches to single-photon detection at telecom wavelength, which are summarized here:

1. Optimization of low-noise InGaAs APDs for detection of single photons at telecom wavelengths

This part of the program aims to extend earlier work done by Dr. Joe Campbell's group at UT Austin on ultra-low noise APDs from the regime of conventional telecom applications into the single-photon regime. In earlier work, the UT Austin group used APD devices with very thin multiplication regions to obtain the lowest excess noise and the highest gain-bandwidth products reported for any APD. They showed, both experimentally [1–4] and theoretically [5], that the low noise is due to the non-local nature of the impact ionization process and the fact that non-locality becomes a dominant effect in very thin high-field regions. In addition, they achieved ultra-low noise operation by using heterojunctions to provide greater localization of impact ionization than can be achieved in spatially uniform structures. This approach they call "impact ionization engineering" or

I²E. The initial demonstration of this concept used the GaAs/$Al_xGa_{1-x}As$ material system; under this program, the concept is being extended to the "long-wavelength" materials that are widely used for fiber optic communications.

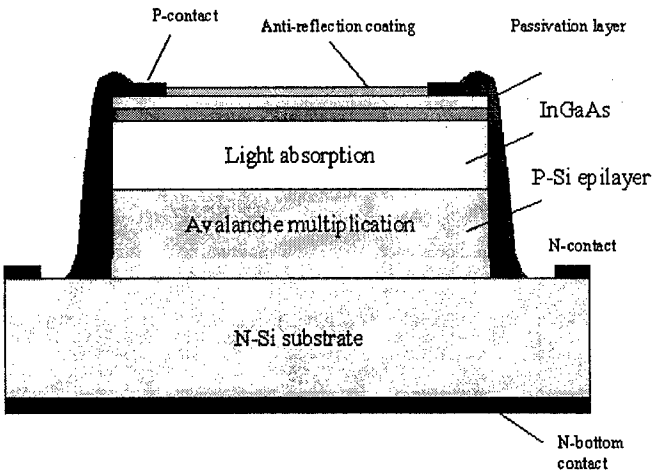

Figure 1. Schematic cross-section of a separate hetero-interface photodetector (SHIP)

2. Development of Si/InGaAs "Separate Hetero Interface Photodetectors"

The second approach to high-efficiency, low-noise detection being pursued under this project is the "separate hetero-interface photodetector (SHIP)," which combines a long-wavelength absorption region with a separate low-noise multiplication region made from a heterogeneous material (Figure 1). For example, this type of structure has been successfully demonstrated using an $In_{0.53}Ga_{0.47}As$ absorber and a Si multiplication region joined together by fusion bonding [6]. We believe that devices based on this approach may be capable of operating as single-photon detectors at temperatures near room temperature or requiring only modest thermoelectric cooling.

Earlier work on InGaAs/Si APDs in Dr Yu-Hwa Lo's group at UCSD and at Nova-Crystals, Inc. (the industrial partner of the UCSD group) has focused on two important aspects for optical communications, namely high gain-bandwidth product and low operation voltage. Under this program, the emphasis is on reduction of the dark current and improvement of the noise figure. It was expected that InGaAs/Si heterostructure APDs can achieve the theoretical limit of the dark current with (1) improved device processing, (2) improved wafer fusion interface, and (3) optimized epitaxial layer structure. Specific goals of this part of the project at the outset of the program included replacing the mesa structure of earlier designs with a planar structure with guard rings; applying a low temperature fusion process in high vacuum will to replace the previously-used high temperature, atmosphere fusion process; and using an optimized doping profile to minimize the tunneling current and to facilitate carrier transport.

3. Nonlinear frequency upconversion and silicon APDs

A third approach that is being explored for detection of single 1.31/1.55-μm photons at or near room temperature uses nonlinear optical techniques to upconvert telecom wavelength photons to a visible wavelength; then low-dark-count, high quantum effi-

ciency Si APDs can be used to detect the upconverted photon (Figure 2). For example, by using sum-frequency generation in a nonlinear crystal, it is possible to mix a single 1.55-μm photon with a strong 1.3-μm pump photon to create a single photon at 0.71 μm, a wavelength that can be detected efficiently using a Si APD. Since Si APDs are (relatively) insensitive to 1.3/1.55 μm, it should be possible to provide sufficient filtering so that only the generated 0.71-μm photon triggers an avalanche.

In this portion of the program, we are investigating the feasibility of this approach and, if it is deemed feasible, we will work toward development of a practical prototype detection system. Planned work includes: studying the inherent sensitivity of Si single-photon counting APDs to sub-bandgap light (λ<1 μm) to evaluate filtering requirements,

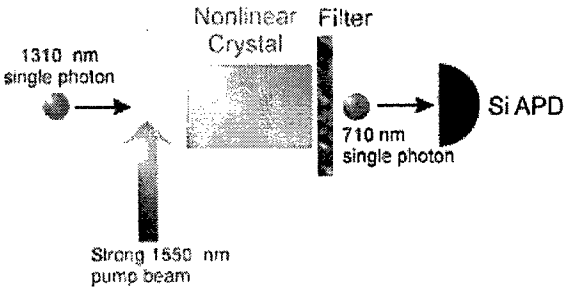

Figure 2. Diagram showing the concept for detection of single telecom-wavelength photons using nonlinear frequency conversion.

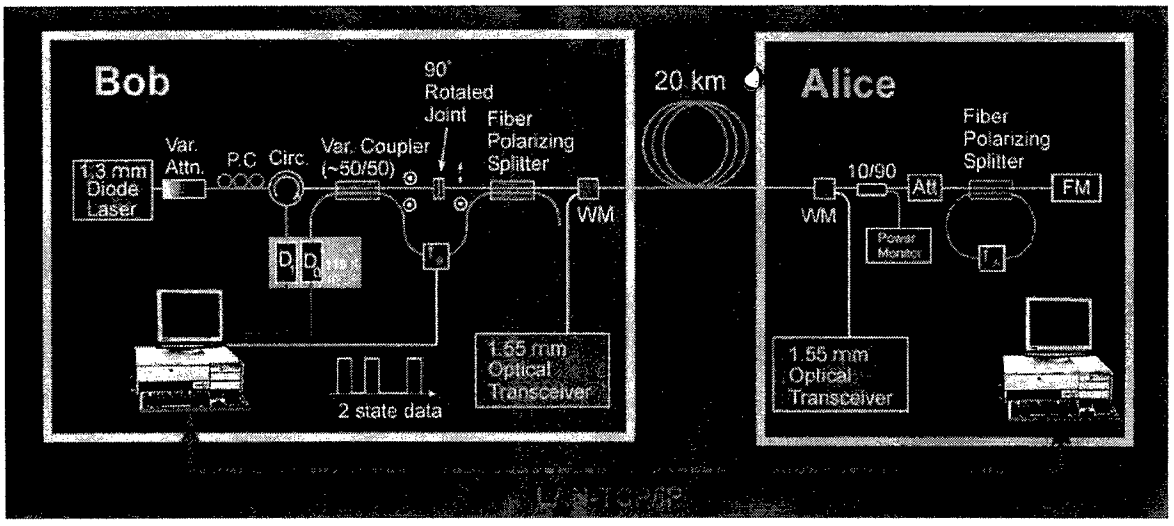

Figure 3. Diagram of the IBM prototype quantum cryptography system.

evaluating possible upconversion schemes compatible with practical nonlinear materials (including periodically-poled materials and waveguide geometries) and pump sources, and comparing performance of such a system to commercially-available Ge and InGaAs APDs and other APDs developed under this program as described above.

Another key aspect of this program involves characterization of the detectors that are

developed using the approaches described above. Quantum key distribution places particular and rather specialized demands on the detectors; "good" performance is defined rather differently than in conventional telecom applications. It is therefore necessary to characterize detectors in a way that fairly evaluates the characteristics that are relevant to quantum cryptography. Hence, one role of IBM group is to characterize any candidate detectors in a manner consistent with similar measurements that they previously performed on commercially-available detectors and to evaluate the performance of promising devices in the IBM prototype quantum cryptography system (Figure 3) [7].

II. Third Year Progress

A. IBM Almaden Research Center Research Prototype Single Photon Detector

1. Introduction

Detection of single photons at telecom wavelengths for quantum cryptography requires not only the detector element itself (typically an InGaAs avalanche photodiode), but also a constellation of specialized electronic elements. This auxiliary electronic circuitry performs a number of crucial functions (Figure 4). It generates a short (~1 ns) bias pulse which, when combined with a DC bias voltage applied to the APD, momentarily biases the APD above breakdown, enabling it to produce an avalanche in response to absorption of a single

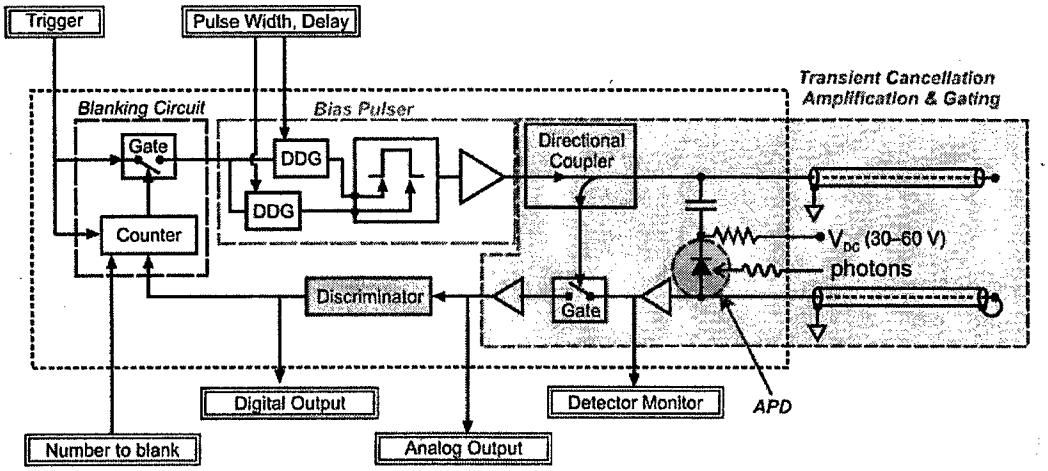

Figure 4. Block diagram showing the functions that must be performed by the auxiliary electronics in order to enable an avalanche photodiode to detect single photons.

photon. However, applying such a short pulse to the capacitive diode generates a transient current that can exceed the current resulting from the avalanche. Thus, the supporting electronics must also separate the photon-induced signal from the capacitive transient. In the IBM prototype QKD system, we use a patented balanced cancellation scheme (US

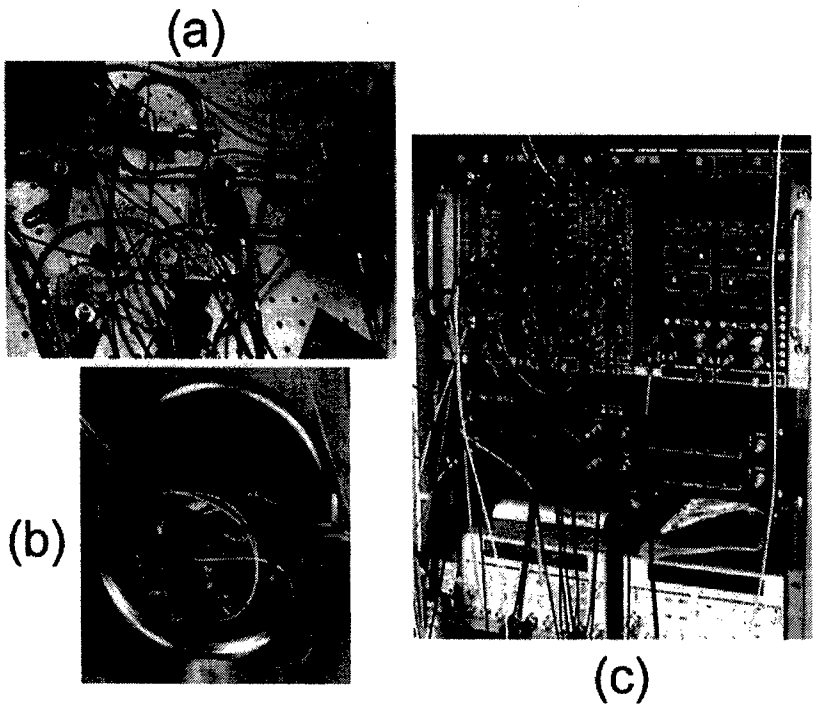

Figure 5. Laboratory apparatus used in earlier detector characterization work. (a) Electronic gating implemented with Minicircuits modules, (b) liquid nitrogen dewar and heater used for temperature control, (c) NIM instruments used for signal processing, discrimination, counting.

#6,218,657) that employs matched transmission lines to create an inverted copy of the transient and subtract it from the "photon+transient" signal, leaving the photon-induced signal against a flat, quiet background. The surrounding electronics must also include a discriminator and amplifiers to generate a logic output pulse when the photon-induced

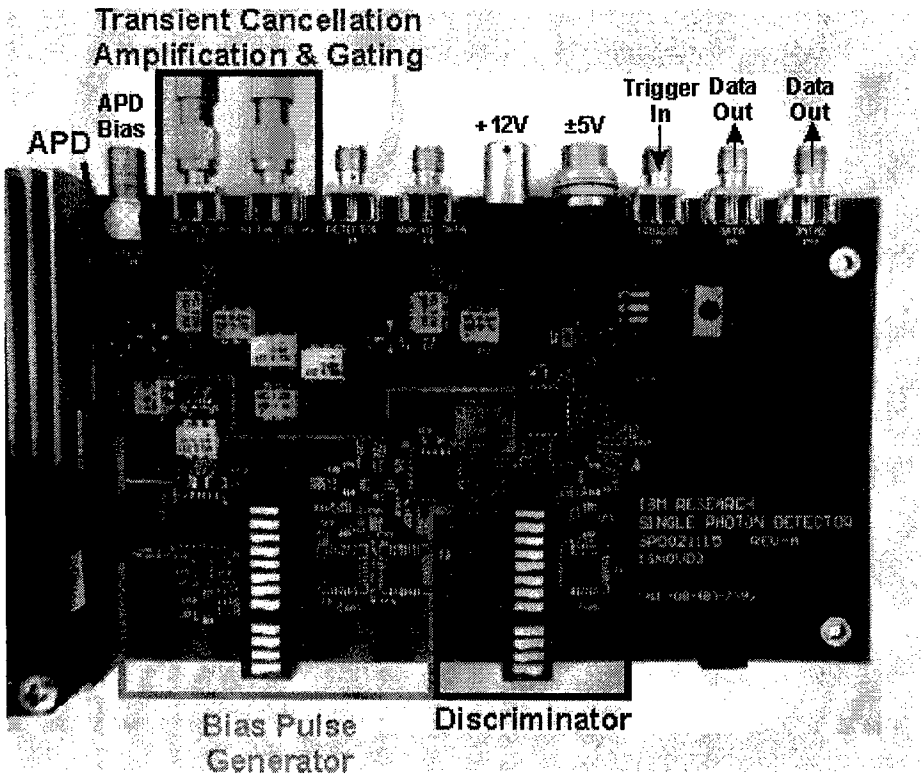

Figure 6. Photograph of the PCB-SPD showing the clusters of components that implement the functions shown in Figure 4.

pulse exceeds a set threshold. In the IBM prototype QKD system and in a separate system we subsequently built for detector characterization [8], these functions were performed by discrete Minicircuits RF modules (Figure 5(a)), a liquid nitrogen dewar / heater combination for varying the temperature (Figure 5(b)) and NIM and stand-alone laboratory instruments (Figure 5(c)).

2. IBM ARC Research Prototype Single Photon Detector

One of IBM's roles in this program has been to enable our university partners to make measurements of single-photon detection efficiency on the novel devices they are developing that can be compared directly with those made previously by IBM on commercially-available InGaAs APDs, so that the new devices developed under this program can be fairly compared with those used in earlier work. Transfer to the universities of the IBM system for single-photon detector characterization proved cumbersome because of the complexity of our original discrete-element laboratory implementation. In order to remedy this situation, in Year Two we developed an integrated printed-circuit-board (PCB) version (Figure 6) of the single-photon detection system (SPD) that contained the electronic elements previously implemented using conventional discrete components. The use of modern surface-mount components and multi-layer PCB techniques made this a very compact and robust replacement for our earlier implementation.

Although this system was originally intended only for use by ourselves and our sub-contractors at UCSD and UTA, great interest was expressed by other DARPA QuIST participants in having versions of this system for their ongoing work under this program. In response to this interest, IBM undertook to provide a limited number of research prototype units to DARPA QuIST participants.

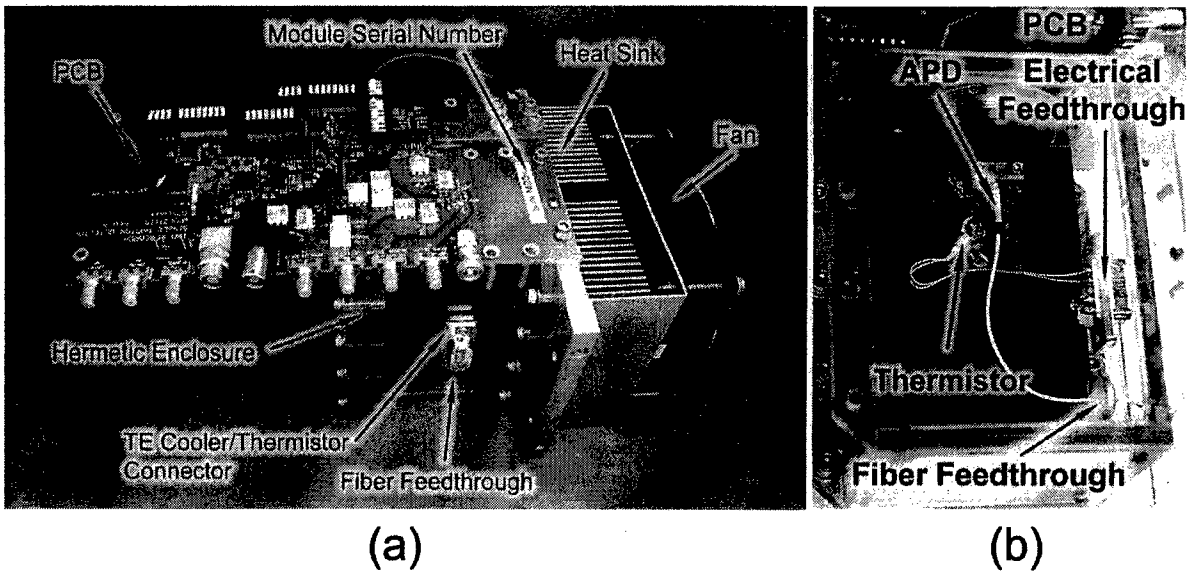

Figure 7 (a) PCB attached to APD module and fan. The hermetic enclosure surrounds an APD affixed to a TE cooler, which can be seen in more detail in (b), where the cover of the module has been removed

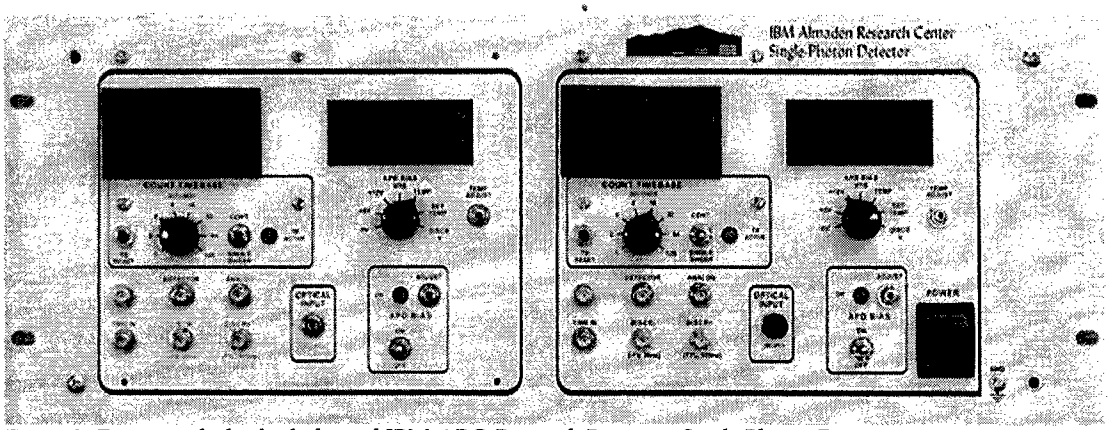

Figure 8. Front panel of a dual-channel IBM ARC Research Prototype Single Photon Detector.

In order to provide a minimum level of self-sufficient operation, the research prototype version of the PCB-SPD included not only the PCB itself, but the APD affixed to a four-stage thermoelectric cooler and mounted inside a hermetically-sealed, insulated module (Figure 7). One or two of these modules were supplied in a 19-inch rackmount chassis with the power supplies necessary to run the units. Control and indicators essential to operation of the unit were brought out to the front panel (Figure 8). A rudimentary interface allowing the DC bias voltage and the temperature set point to be set remotely via computer was also provided.

The completed units offered a number of features:

- The instrument internally provides a 4.5-V bias pulse with length settable between 0.8 ns and 5 ns.
- The delay between the input trigger and the bias pulse can be adjusted over a range of ~10 ns in 10 ps steps.
- An on-board discriminator produces an output logic pulse when the detected APD signal exceeds a value that can be set by the user.
- The APD can be cooled to ~210K by the integrated four-stage thermoelectric cooler and controller.
- A built-in counter records the number of counts; the count interval can be set from 1-256 seconds (2^n seconds, where $0 \leqslant n \leqslant 8$).
- A front panel meter allows monitoring of power supply voltages, bias voltage, actual temperature, temperature setpoint, and discriminator threshold.
- An on-board blanking circuit can be used to suppress a set number of bias pulses (0-255), which helps suppress false counts caused by afterpulsing. (We found that a setting of ~6, corresponding to a 12-μs dead time, was sufficient to gain most of the benefit without unduly increasing the risk of missing a desired pulse.) This feature was added during a revision to the PCB done during Year Three—it was not present in the basic PCB design reported in the Year Two Progress Report and shown in Figure 6 of this report.

The user manual describing the instrument and its operation in greater detail has been included as Appendix A.

We built a total of 30 single-photon detector modules. Some of these were placed into single channel instruments; others in dual channel instruments (such as that shown in Figure 8). The breakdown and disposition of these units is given in Table I.

Recipient	Singles	Duals
BBN	—	5
Boston University	—	2
JPL	—	1
Johns Hopkins University	2	—
NIST	1	—
LTS-Telcordia	2	—
UCSD	1	—
UTA	1	—
IBM	1	3

Table I. Summary of disposition of IBM ARC PCB-SPD units

The units delivered to BBN and Boston University have already been integrated into the DARPA Quantum Cryptography Network in the Boston/Cambridge area. BBN reports that replacement of the detectors they previously used with the IBM ARC prototype significantly improved the performance of their system (Figure 9).

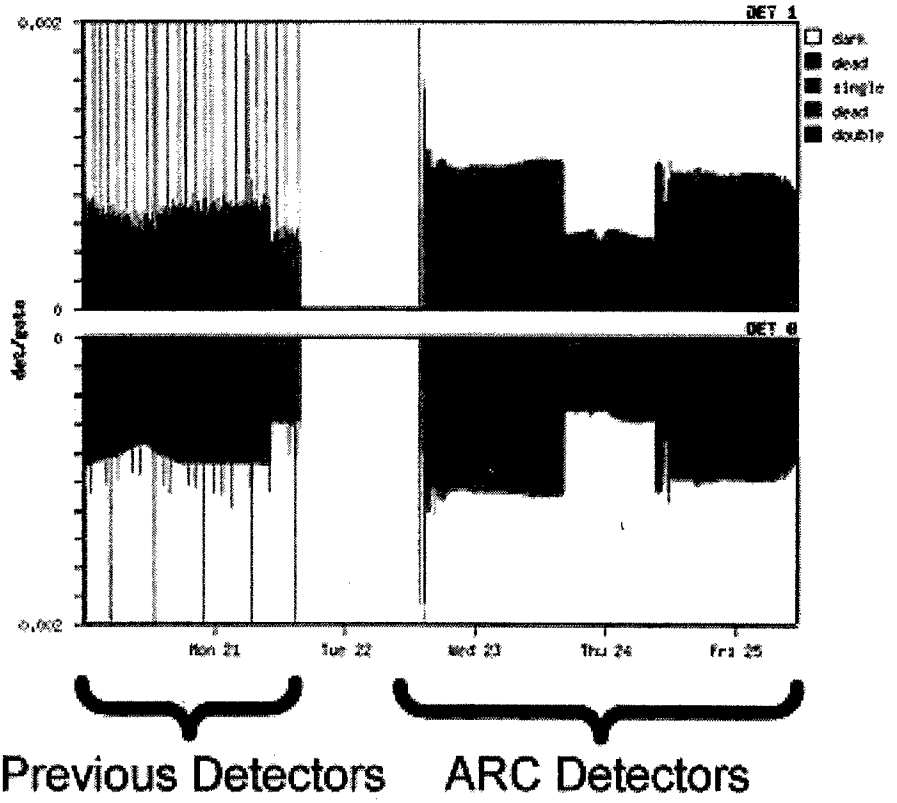

Figure 9. Record of detection events in the BBN quantum cryptography system. Higher bits rates with less noise were achieved when the previously-used detectors were replaced by the IBM ARC Research Prototype PCB-SPD. The recording apparatus is run continuously; this explains the dead time and variations in bit rate as various aspects of the system are adjusted.

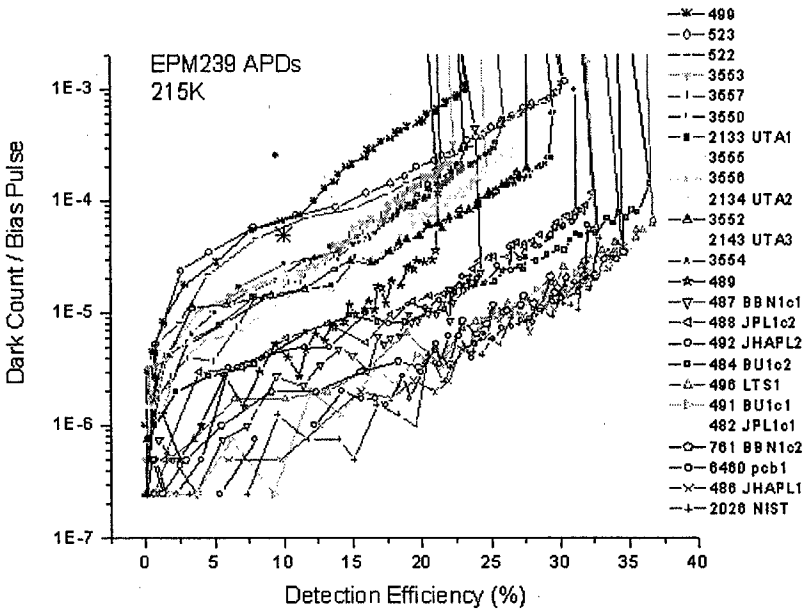

Figure 10. Dark counts per bias pulse vs. detection efficiency for several EPM239 APDs

3. Further characterization of EPM 239 APDs

The APD included in the IBM ARC Research Prototype PCB-SPD is the JDSU/Epitaxx EPM239. This detector has been the "workhorse" most widely used in quantum cryptography research and development for the past several years.

In order to deliver prototypes with the best possible performance, we screened a large number (>50) of EPM239's. The data gleaned from this process sheds further light on the variability of these detectors when used for single-photon counting and on the need for improvements in basic detector technology (as has been pursued by UTA and UCSD under this program).

As shown in Figure 10, there is a wide variation in the performance characteristics of these detectors when cooled to 215K and transiently biased above breakdown. When used as intended—at room temperature and under appropriate bias—the performance is uniformly good. This is not surprising, considering that these devices were produced to meet specifications for conventional telecom applications and not for single-photon counting.

This accumulation of this much data on the performance of EPM239's enables us to look for correlations between the performance of these devices in single-photon-counting mode and the parameters that are traditionally characterized and specified, such as room-temperature reverse breakdown voltage.

As shown in Figure 11(a), there does appear to be a correlation between dark counts/bias pulse in single-photon mode and reverse breakdown voltage. According to Figure 11(b), there is not a similar correlation with afterpulse probability, which seems to be essentially independent of reverse breakdown voltage.

The structure of this device (Figure 12) may reveal a reason. The highlighted region shows

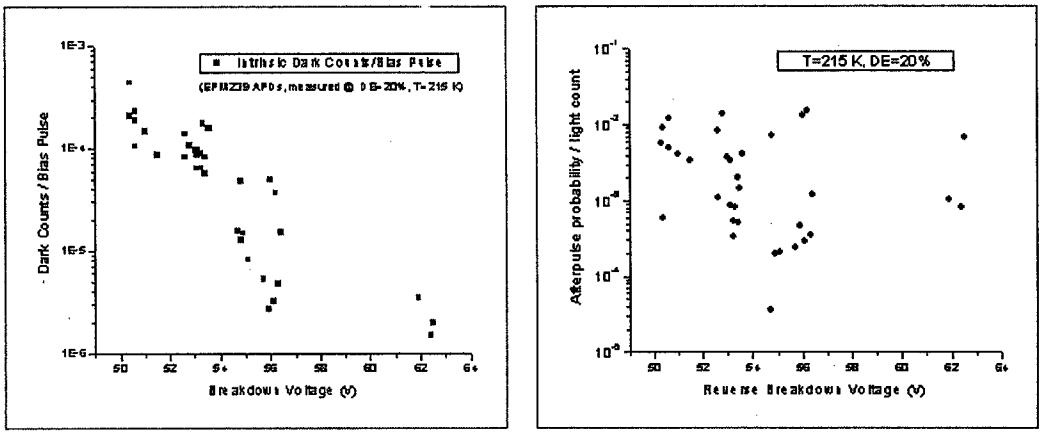

Figure 11. (a) Dark counts/bias pulse vs. reverse breakdown voltage corresponding to the APDs in Figure 10. (b) Afterpulse probability vs. reverse breakdown voltage corresponding to the APDs in Figure 10.

where avalanche multiplication occurs. In the Epitaxx device, the thickness of this region is determined by a zinc double diffusion rather than by epitaxy. An advantage of using a diffusion process is that the lateral extent of the region is also defined, whereas if the layer thickness were defined by epitaxy, the lateral extent would be defined by etching a mesa, which can create surface states that contribute to dark current. A disadvantage of using diffusion is that this process produces variations in the thickness of the layer.

In order to increase the speed of devices like this for telecom applications, the thickness of the layers shown in Figure 12 has been progressively reduced. This reduction has the adverse effect of reducing the absorption, increasing the probability of tunneling, and reducing the breakdown voltage, which, according to the data of Figure 11, increases the dark count rate.

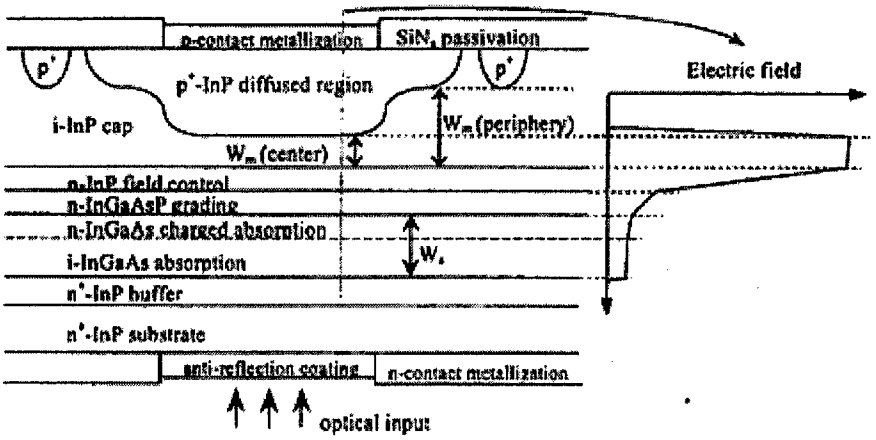

Figure 12. APD device structure and electric field profile in the center of the avalanche region (taken from M. A. Itzler, et al., "High-performance, manufacturable avalanche photodiodes for 10Gb/s optical receivers," Optical Fiber Communications Conference 2000, Volume 4, 7–10 March 2000, pp. 126–128.

4. Conclusions

The IBM ARC Research Prototype PCB-SPD has been provided to several DARPA participants. The feedback from initial use of these instruments in quantum cryptography systems has been very positive. It is clear that the continued development of practical quantum cryptography systems depends on the availability of good telecom-wavelength single-photon detectors. Both the light-sensitive element itself and the constellation of electronics surrounding it must be optimized for best performance in the single photon regime. IBM is actively seeking to license this technology to a partner who can continue to make it available to the quantum cryptography community.

B. Separate Hetero-Interface (Si/InGaAs) Photodetectors

The research of the UCSD team has been focused on four areas related to single-photon APD detectors for quantum cryptography:

1. investigation of theafterpulsing effect,
2. development of physical models for dark count and single-photon detection efficiency,
3. demonstration of InGaAs-on-Si single-photon detectors, and
4. understanding of APD response to different input photon numbers.

Results from these four research tasks significantly advance our understanding of and ability to fabricate single-photon APDs at telecom wavelengths.

1. Investigation of afterpulsing effect for single-photon avalanche detectors

Summary:

The impact of the afterpulsing effect and its temperature dependence were studied both experimentally and theoretically. The primary dark current and detrap time as functions of temperature were obtained by fitting the experimental data. The result unequivocally reveals the impact of afterpulsing effect on the dark count rate. An optimum operation temperature for low dark count operation was observed for single-photon avalanche detectors (SPADs).

Detailed Discussion:

When biased above breakdown (Geiger mode condition), an avalanche photodiode (APD) can produce a tremendous gain (10^7–10^8) within a time window of a few nanoseconds. Such Geiger-mode APDs must have a high detection efficiency for single photons while keeping the dark count probability low. Unfortunately, the implementation of III-V APDs as Geiger-mode APDs at wavelengths beyond 1 μm is hindered by high dark count rate. Cooling can be used to reduce the dark count rate; however, with InGaAs/InP APDs cooling usually worsens the afterpulsing effect. Afterpulses occur when carriers are released from traps in the multiplica-

tion region and successfully trigger avalanche breakdown. The afterpulsing effect can seriously degrade the performance of the APD and limit the operation rate for photon counting.

A commercial InGaAs/InP APD (Epitaxx EPM239AA) was used to study the afterpulsing effect. A laser, synchronized with a voltage pulse generator, was fired at a repetition rate of 50 kHz to generate short light pulses at the wavelength of 1.3 μm. By using a variable attenuator, the optical energy per pulse delivered to the APD was reduced such that the average number of photons per pulse was 0.3. The actual number of photons within each pulse follows a Poisson distribution. The voltage pulse generator sent square pulses to the APD at 100 kHz (coincident with and between the light pulses, as shown in Fig. 13 (a) and (b)). These pulses, superimposed on a DC bias, brought the reverse bias above V_B for 2 ns. The diode under test was mounted on a temperature-controlled plate in a cryostat. A simple transient-canceling circuit was used to separate the avalanche current pulses from the capacitive transient pulse at the diode output. Finally, the avalanche current pulses were registered by a counter.

When the laser light was off, there should be no difference between the count probability of coincident and interleaved pulses. The measured dark count rate for the interleaved pulses is shown in Fig. 14 (▲). When the laser light was on, the counts for coincident and interleaved pulses were registered separately. Since the coincident pulses had light input, there was a higher chance of avalanche for those pulses than for the (dark) interleaved pulses. The count rate for coincident pulses, shown in Fig. 14 (♦), is almost constant throughout the entire temperature range of measurement. What is most noticeable is the temperature dependence of the count rate for the interleaved pulses, shown in Fig. 14 (□). The count rate for the interleaved pulses is close to the count rate when the laser light was off only at higher temperatures. After the initial decreasing trend with decreasing temperature, the count rate for the interleaved pulses starts to increase when temperature decreases further. Hence, there is an optimum operating temperature. The difference between the dark count rate and the count rate of the interleaved pulses when the light was on gives a measure of the probability of afterpulsing due to the effect of carrier trapping.

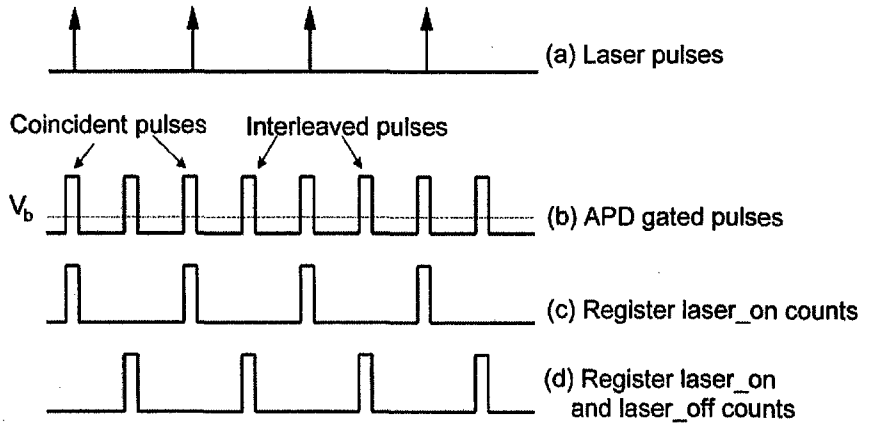

Figure 13. Diagram indicating the different synchronization arrangements used in the measurements.

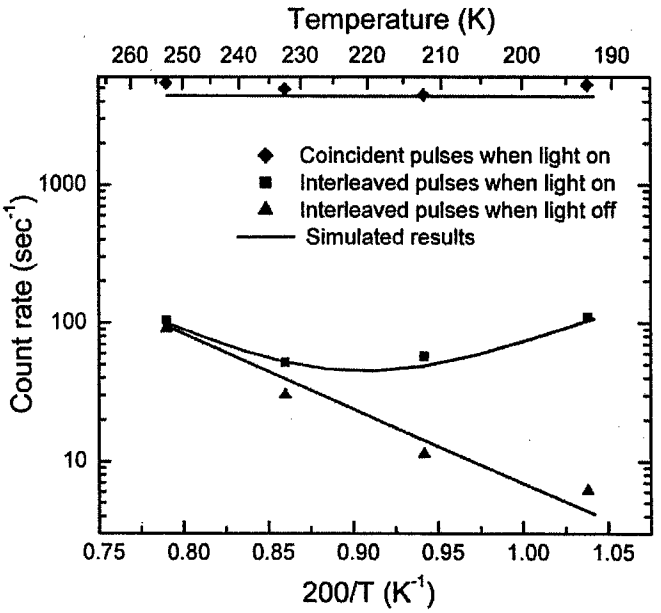

Figure 14. Count rates vs. temperature. Symbol lines correspond to measured data using Epitaxx EPM239AA APD: ♦ counts registered for coincident pulses when light was on, □ counts registered for interleaved pulses when light was on, and ▲ counts registered for interleaved pulses when light was off. Continuous lines are simulated results fitting the experimental data.

The dark count probability (Fig. 14 (▲)) has a strong dependence on the temperature. This dependence arises because the dark counts are mainly triggered by thermally-activated dark carriers, and the activation rate decreases exponentially with temperature. Thus, it would appear that in order to lower that component of the dark count rate induced by primary dark current, the device should be cooled as much as possible. However, low temperature exacerbates the afterpulsing effect because the detrap time of the carriers increases exponentially with reduced temperature. That is why the dark count rate for the interleaved pulses increases for temperatures lower than 220K (Fig. 14 (□)). Fitting the physical model we developed to the experimental data, we obtained the temperature dependences of the primary dark current I_{DM} and the detrap time constant τ_d, as plotted in Figs. 15 and 16, respectively.

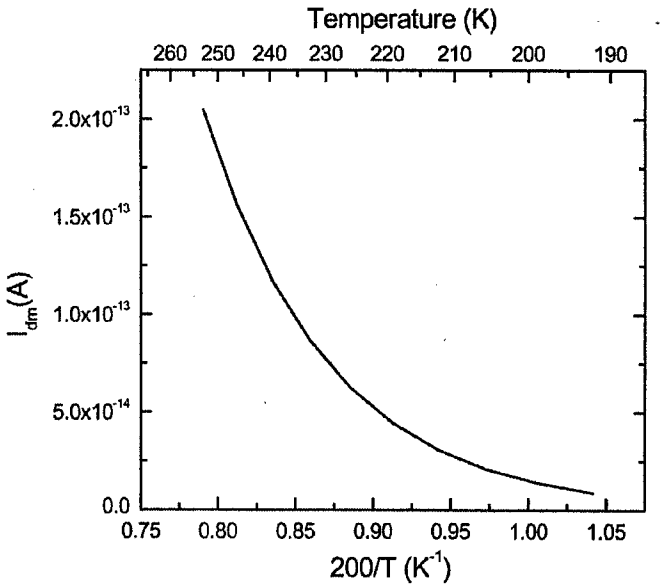

Figure 15. The dependence of primary dark current on temperature used in the curve fitting shown in Fig. 14.

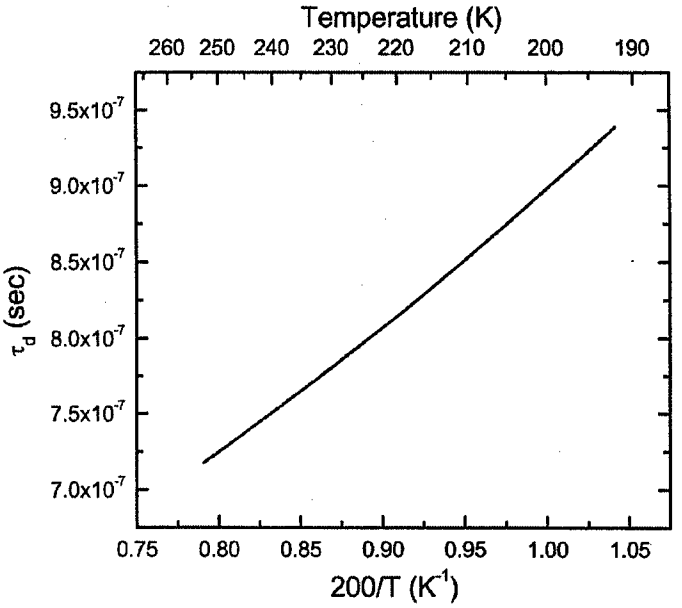

Figure 16. The dependence of detrap time on temperature used in the curve fitting shown in Fig. 14

2. Development of physical models for dark count probability and single-photon quantum efficiency

Summary:

We developed a physical model that quantitatively describes the behavior of the dark count probability and single-photon quantum efficiency. The model enables us to make direct connections between the performance of SPADs and device parameters (e.g. dark current, detrap time, gain-bandwidth product, etc.) and operating conditions (e.g. dc gain, Geiger mode gain, gate repetition rate, etc.). Such information is useful for selecting and designing APDs for single-photon detection, as well as understanding device behavior under operating conditions that allow single-photon detection. The theory agrees well with the experimental results.

Detailed Discussion:

For single-photon detection, a SPAD is usually dc-biased a few volts below its breakdown voltage V_B, and is periodically pulse-biased above V_B for a short time. If a photoexcited carrier is present during this time, an avalanche process may be initiated to produce a current pulse on the order of milliamperes, corresponding to a Geiger mode gain M_g of $10^6 - 10^8$. Ideally, SPADs should produce no current response under dark conditions. However in practice, the seed carriers can be generated not only by optical excitations but also by other mechanisms, such as primary dark current and carriers released from the traps in the multiplication region. The primary dark current is defined as the dark current that flows through the same multiplication region of a SPAD as the photocurrent does, measured at the unity gain condition. Because dark count prob-

ability P_d and single-photon quantum efficiency (*SPQE*) are two most important figures of merit of SPADs, our analysis will focus on these two quantities.

To create a dark count, two statistically independent events have to happen: (a) dark carriers are generated and (b) the avalanche process has to be triggered. Assuming N_d is the average number of dark carriers in the multiplication region and P_a is the probability of triggering the avalanche event above the threshold M_g by each carrier, the probability of dark count, P_d following the Poisson statistics can be represented as

$$P_d = 1 - \exp(-N_d P_a) \tag{1}$$

Eq. (1) represents the probability that at least one dark carrier successfully triggers an avalanche. There exist four distinct mechanisms in a SPAD that can contribute to N_d.

1) *Primary dark carriers injected or generated inside the multiplication region during the voltage pulse.* The magnitude can be represented as:

$$N_{DM1} = I_{DM}\tau / q \tag{2}$$

where I_{DM} is the primary dark current, τ is the gate pulse width, and q is the charge of an electron.

2) *Dark carriers generated before the voltage pulse.* Since the bias voltage prior to the pulse is only about a few volts (e.g. 1–2V) below V_B, primary dark carriers generated before the arrival of a bias pulse can go through a series of impact ionizations with an average dc gain of M_0. Due to the finite frequency response of the SPAD, some carriers may still remain in the multiplication region when the voltage pulse arrives, and therefore can be treated as seed carriers. The average number of dark carriers thus generated is given by

$$N_{DM2} = I_{DM} M_o \tau_{tr}^* / q \tag{3}$$

where τ_{tr}^* is the effective transit time. With a multiplication gain larger than the reciprocal of ionization coefficient ratio, i.e. when $M_o k > 1$, APDs exhibit a constant gain-bandwidth product GB. τ_{tr}^* is then dominated by the avalanche buildup process, and can be approximated by $\tau_{tr}^* = M_o / 2\pi GB$, where GB is the gain-bandwidth product of the SPAD.

3) *Dark carriers arising from the release of trapped carriers during the voltage pulse.* These carriers could have been trapped during any of the previous current pulses and this effect is commonly called afterpulsing. It is assumed that the probability of carriers escaping from the traps follows an exponential function with a characteristic detrap time constant τ_d; and the average number of carriers trapped after a current pulse is $N_{tr} = cM_g / (1-c)$, where c is the ratio of the trapped carriers to the total carriers generated per avalanche pulse and its value depends on the number of unfilled traps in the multiplication region. The average number of detrapped carriers within the duration of the voltage pulse τ is

$$N_{t1} = P_d N_{tr} \sum_{n}^{\infty} \left[\exp\left(-\frac{n\Delta T - \tau}{\tau_d} \right) - \exp\left(-\frac{n\Delta T}{\tau_d} \right) \right] = P_d N_{tr} \frac{\exp(\tau/\tau_d) - 1}{\exp(\Delta T/\tau_d) - 1} \tag{4}$$

where ΔT is the reciprocal of the pulse repetition rate.

4) *Based on a argument similar to that in 2), carriers released from the traps before the voltage pulse may also stay in the multiplication region when the voltage pulse arrives.* The number of such dark carriers can be written as

$$N_{t2} = P_d N_{tr} \sum_{n}^{\infty} \left[\exp\left(-\frac{n\Delta T - \tau_{tr}^*}{\tau_d} \right) - \exp\left(-\frac{n\Delta T}{\tau_d} \right) \right] = P_d N_{tr} \frac{\exp(\tau_{tr}^*/\tau_d) - 1}{\exp(\Delta T/\tau_d) - 1} \tag{5}$$

Figure
detrap
extract

Finally, the total number of dark carriers per pulse in a SPAD is the sum of these four sources, so

$$N_d = N_{DM1} + N_{DM2} + N_{t1} + N_{t2} \tag{6}$$

Another important parameter for the dark count calculation is the probability for a carrier to cause an avalanche, P_a. McIntyre has theoretically calculated P_a's of electrons and holes as functions of the ionization coefficient ratio k and $\delta = \int \alpha \, dx$ (α : ionization coefficient for electrons). Here we treat P_a as a parameter so our results are applicable to any APDs without being restricted to a particular device structure or electric field distribution in the multiplication region.

Substituting Eqs. (2)–(6) into Eq. (1), the dark count probability P_d is given by

$$P_d = 1 - \exp\left\{ -P_a \left[\frac{I_{DM}\tau}{q} + \frac{I_{DM} M_0^{\,2}}{2\pi q G B} + P_d N_{tr} \frac{\exp(\tau/\tau_d) - 1}{\exp(\Delta T/\tau_d) - 1} + P_d N_{tr} \frac{\exp(\tau_{tr}^*/\tau_d) - 1}{\exp(\Delta T/\tau_d) - 1} \right] \right\} \tag{7}$$

Because P_d appears in both sides of Eq.(7), this equation must be solved numerically.

The *SPQE*, also known as detection efficiency, is commonly defined as

$$SPQE = (P_{on} - P_d)/P_{ph} \tag{8}$$

where P_{on} is the probability of a current pulse triggered by either a photon-generated carrier or a dark carrier when the single-photon source is on; and $P_{ph} = 1 - e^{-N_0}$ is the probability that an incident optical pulse contains at least one photon with the average number of photons per pulse N_0. Although this is a commonly accepted definition of *SPQE*, we should point out that Eq. (8) describes the true single-photon quantum efficiency only when the error rate due to afterpulse is relatively low. Otherwise, Eq. (8) tends to overestimate *SPQE*.

The method of calculating P_{on} is similar to the calculation of the dark count probability, P_d, except that the effect of optical input has to be considered. Accordingly, Eqs. (1) and (6) should be modified as

$$P_{on} = 1 - e^{-N_{on}P_a} \tag{9}$$

$$N_{on} = N_{DM1} + N_{DM2} + N'_{t1} + N'_{t2} + \eta N_0 \tag{10}$$

where η is the conventional quantum efficiency of a detector, determined by the absorption coefficient and the thickness of the absorption layer. Equations (4) and (5) can still be used for N'_{t1} and N'_{t2}, except that P_d should be replaced by P_{on}. The additional term in Eq. (10), ηN_0, accounts for the optical induced carriers. The final expression of P_{on} is then given by

$$P_{on} = 1 - \exp\left\{-P_a\left[\frac{I_{DM}\tau}{q} + \frac{I_{DM}M_0^{\,2}}{2\pi qGB} + P_{on}N_{tr}\frac{\exp(\tau/\tau_d)-1}{\exp(\Delta T/\tau_d)-1} + P_{on}N_{tr}\frac{\exp(\tau^*_{tr}/\tau_d)-1}{\exp(\Delta T/\tau_d)-1} + \eta N_0)\right]\right\} \tag{11}$$

Finally, the *SPQE* can be calculated from Eqs. (8) and (11).

The above analysis shows explicitly how dark count and *SPQE* depend on different device parameters and operating conditions. In the following, we will use calculated results to illustrate the effects of the major parameters. The dependence of P_d as a function of *SPQE* is shown in Figure 17 for different I_{DM} (0.1, 1 and 10 pA), assuming that afterpulsing is negligible, which is reasonable given $\tau_d \ll \Delta T$. Note the strong effect of primary dark current on the dark count probability. The calculation agrees very well with the measured results obtained from commercial APDs (EG&G InGaAs APD at 240 K with measured I_{DM} of 5pA and NEC NDL3351P APD at 130 K with measured I_{DM} of 0.1 pA), as shown in Fig. 17. The same measurement conditions were used in the calculation shown in Fig. 17. In the region of high quantum efficiency, the

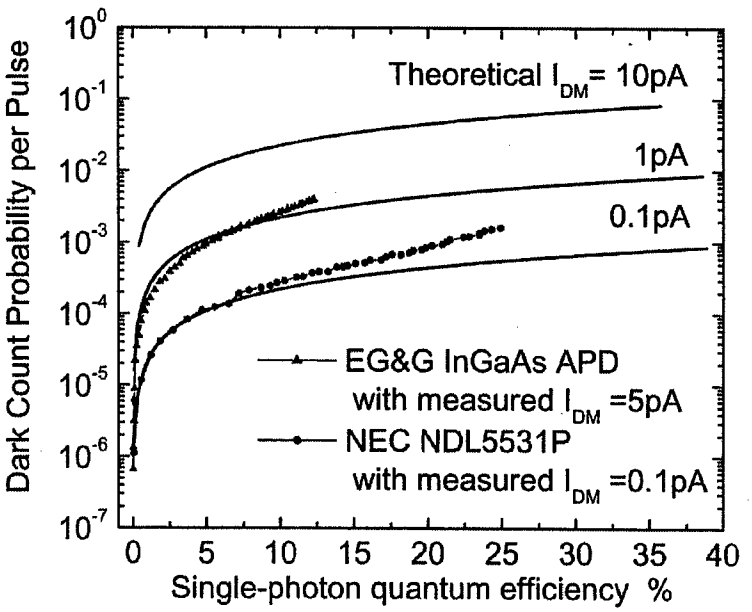

Figure 17. Calculated (solid lines) and measured (symbol lines) dark count probability vs. single-photon quantum efficiency for different I_{DM}. Other parameters are: $f = 1/\Delta T$ = 100kHz, pulse width τ = 2ns, τ_d = 200 ns, c is 1%, N_0 = 0.3 photon/pulse, M_g = 10^8, and GB = 30GHz.

measured dark count increases more rapidly than the model. This is because the dc bias voltage and therefore M_0 increases in the measurement in order to reach the high *SPQE*, whereas our calculation has kept the dc bias and M_0 constant.

The effect of the dc gain M_0 is shown in Fig. 18 for SPADs with different gain-bandwidth products. Here the I_{DM} is assumed to be 0.1pA, and all the other parameters are kept the same as in Fig. 17. M_0 affects P_d through N_{DM2} as shown in Eq. (3) – a higher M_0 yields a larger P_d. The results from Figs. 17 and 18 suggest that low primary dark current and low dc bias gain are important for achieving a low dark count or equivalently a high single-photon quantum efficiency at a given dark count.

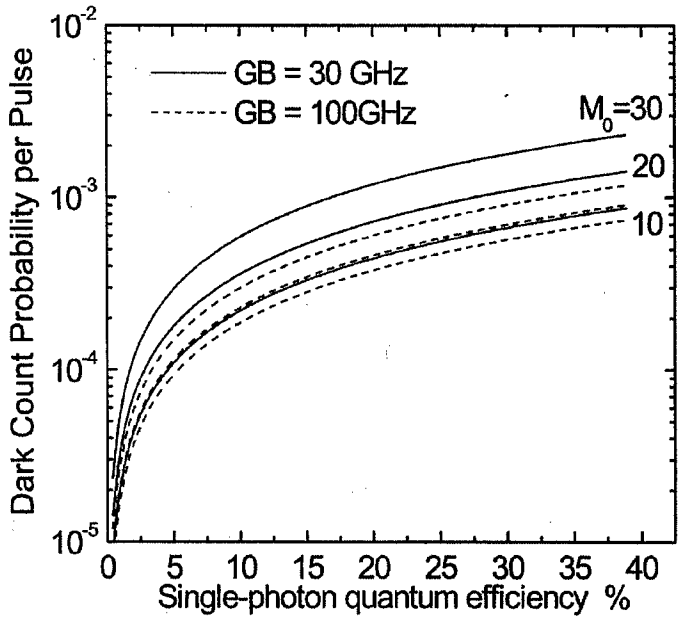

Figure 18. Calculated dark count probability vs. single-photon quantum efficiency for three different M_0 levels. The solid lines indicate APDs with GB of 30 GHz; the dashed lines indicate APDs with GB of 100 GHz. The detrap time constant is set much smaller than the time period between pulses, so that the afterpulse effect is almost negligible in this calculation.

Experimental results have also shown that the afterpulse contribution to the measured counts is negligible at low pulse repetition rate. This can be clearly explained from the last two terms in the product of Eq. (7). When all the trapped carriers are released before the next voltage pulse arrives, the chance of afterpulsing is minimal. Experimentally, Si SPADs have exhibited weak trapping with very small τ_d (~10 ns at room temperature). In contrast, τ_d for III/V APDs is typically hundreds of nanoseconds or microseconds at room temperature and, in addition, the latter devices have a higher trap density in the III/V multiplication region. As the device is cooled to achieve low primary dark current, τ_d for III/V APDs increases, causing a more serious afterpulsing effect. In Figure 19(a), the relative contribution of afterpulse to the total dark count is plotted against the pulse repetition rate with different detrap times, τ_d. Clearly the contribution of afterpulse increases rapidly and becomes dominant once the repetition rate reaches a certain threshold value. Figure19(b) plots the voltage pulse period ($=1/f$) for which the afterpulse contribution reaches 1% of the total dark count versus τ_d for different M_g. We conclude that to keep the afterpulse at a negligible level, two conditions should be satisfied: (1) the voltage pulse

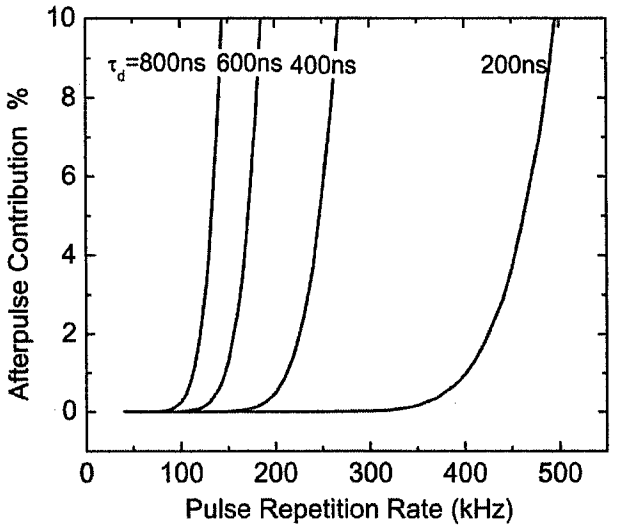

(a)

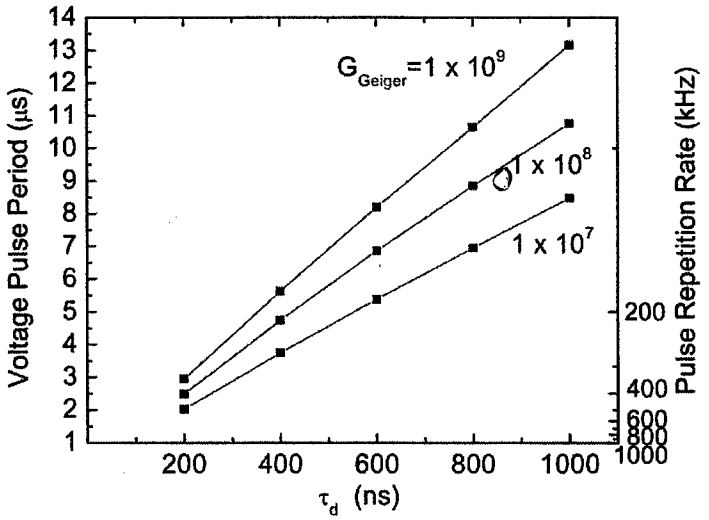

(b)

Figure 19. (a) Contribution of afterpulses to dark counts vs. pulse repetition rate for different detrap time constants with $M_g = 10^8$. *(b) Voltage pulse period (1/f) at which the contribution of afterpulses to dark counts is 1% as a function of* τ_d, *with different Geiger mode gains.* $I_{DM} = 0.1pA$, *SPQE=20% and all the other parameters are the same as Fig. 17.*

period should be at least ten times longer than the detrap time τ_d; (2) a low pulse repetition rate is needed when a higher Geiger mode gain is used for single-photon detection.

3. High-performance InGaAs-on-Si single photon avalanche photodetectors

Summary:

We demonstrated an InGaAs-on-Si single photon avalanche diode (SPAD) with high-single-photon quantum efficiency and low-dark-count probability under gated-mode operation. At 223 K, the device exhibited a dark count probability of $10^{-4} - 10^{-3}$ and a singe-photon quantum efficiency of 33% without anti-reflection coating. The devices also showed high efficiency and low dark count with the smallest normalized excess voltage (4.7% V_{bd}), as a result of the Si multiplication region

Detailed Discussion:

Figure 20 schematically depicts the Separated Absorption and Multiplication (SAM) structure of the InGaAs-on-Si APDs. The device has a light-sensitive diameter of 150 μm and a total-junction diameter of 200 μm.

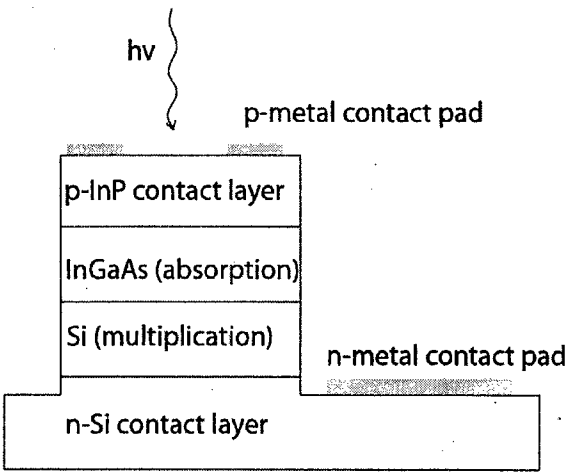

Figure 20. Schematic InGaAs-on-Si SPAD device structure.

Figure 21 shows typical I-V characteristics in the dark and under illumination at 298 K and 223 K. At 223K the dark current at 90% of the breakdown voltage is as low as 20 pA. For the single photon counting experiment the devices were connected on-wafer with high-frequency probes and operated in a gated mode where a train of voltage pulses was superimposed on a DC bias, V_{dc}. The DC bias was set slightly below the device breakdown voltage. The voltage pulse was 2 ns wide and 1.9 V high and had a repetition rate of 100 kHz. A 190 ps optical pulse was generated using a laser pulse source (Hamamatsu C8898) emitting at a wavelength of 1550 nm. The laser pulses were attenuated to an average energy of 0.1 photon/pulse and coupled to the device with a single-mode optical fiber probe. The avalanche pulses produced by the SPAD, caused by photo or dark carriers, were registered with an electronic counter (Stanford Research Systems SR400). A simple voltage transient-canceling circuit was used to separate the avalanche

current pulses from the capacitive transient pulses at the diode output. Both the pulsed laser and the counter were triggered by the voltage pulse generator (Agilent 81110A). The superimposed gated bias, $V_{dc}+V_g$, produced an excess voltage V_e above the APD breakdown voltage, V_{bd}, following the simple relation: $V_e = V_{dc}+V_g-V_{bd}$. In our experiment, the height of the voltage pulse V_g remained fixed at 1.9 V and the excess voltage was varied by changing the DC bias. While V_{dc} was varied from –37.6V to –38.1V, the excess voltage, V_e, was changed from 3.4% to 4.7% V_{bd} ($V_{bd} = -38.2$ V at 223K).

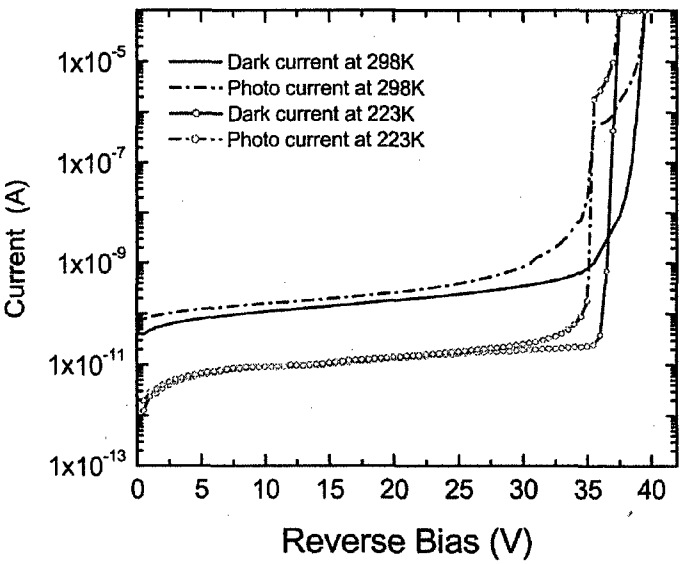

Figure 21. Photo and dark current versus reverse bias of InGaAs-on-Si SPAD at different temperatures.

Dark count probability (P_d) versus single-photon quantum detection efficiency (*SPQE*) of the InGaAs-on-Si SPAD is plotted in Figure 22. Here P_d is defined as the probability of having a count triggered by non-photon-excited carriers during a gate period. P_d was obtained from the ratio of the number of registered counts and the total number of gate pulses when the device was in the dark. The *SPQE* is defined as the probability of having a count triggered by photo-generated carriers during a gating period. At each excess bias level, the *SPQE* was obtained by 1) subtracting the dark count from the total number of registered counts when the laser was turned on and 2) normalizing the result by the number of available photons per pulse. Because the light source was a semiconductor laser, a Poisson distribution for photon number was used to calculate the average number of photons per light pulse. In our measurements the afterpulse effect was negligible because the gate repetition rate (100 kHz) was chosen to be much lower than the escape rate of trapped carriers. If the gate repetition rate was increased substantially, the above method would overestimate the *SPQE* due to the afterpulse effect.

Each data point in Fig. 22 was measured at a corresponding DC bias. Both P_d and *SPQE* increase with the magnitude of the DC bias. When the DC bias voltage, V_{dc}, reaches the break-

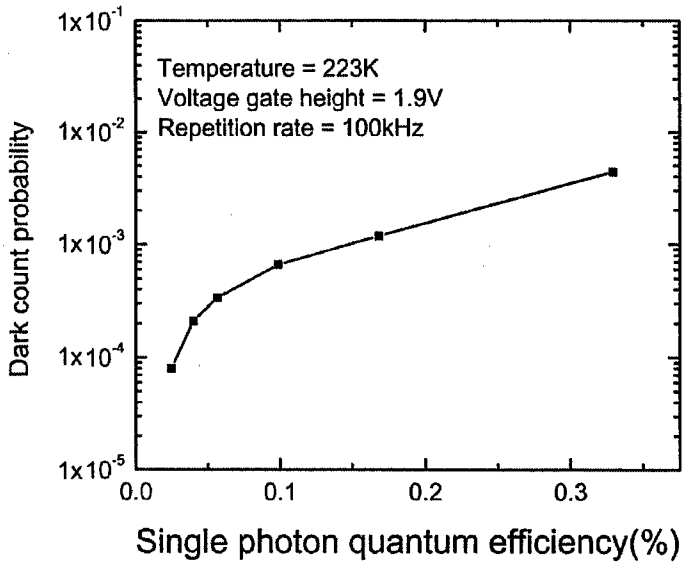

Figure 22. InGaAs-on-Si SPAD dark count probability versus single photon quantum.

down voltage the dark count probability, P_d, experiences an abrupt jump, limiting the maximal *SPQE* that the device can practically achieve. Fig. 22 shows that the dark count probability was in the range of $8\times10^{-5} - 4\times10^{-3}$ when the *SPQE* was between 2.5% and 33%, for a repetition rate of 100 kHz at 223K. This result is comparable to the published results on InGaAs/InP APDs under similar conditions. Note, however, that the commercial APDs used for comparison had a smaller diameter (40 μm). Small APDs are expected to exhibit low dark count probabilities at the same *SPQE*. Because the area of the InGaAs-on-Si SPAD is 25 times larger than of the commercial InGaAs/InP APDs, it is expected to have a more than one order of magnitude improvement if we decrease the device size down to 40 μm. Also, a 40% improvement in SPQE could be achieved using an antireflection coating. Finally it is possible that the results may have been negatively affected by the fact that the measurements were performed on-wafer instead on a packaged device.

Values for the noise equivalent power (NEP) based on single-photon detection were also obtained. Its dependence on the discrimination levels of the pulse counter is shown in Fig. 23. It appears that the NEP remains nearly constant with the DC bias, V_{dc}, up to a certain discrimination level. Above this level the NEP increases dramatically. The minimum NEP for different values of V_{dc} falls in the range of $8\text{-}18\times10^{-16}$ W/Hz$^{1/2}$, which is comparable to the published values for InGaAs/InP SPADs under similar conditions.

One noteworthy feature of the InGaAs-on-Si Geiger-mode SPADs is that the required excess bias to achieve the highest detection efficiency of 33% was only 1.9V (=4.7% V_{bd}). To the best of our knowledge this is by far the smallest excess bias required to obtain such high SPQE while keeping the dark count low. The ability to simultaneously achieve high SPQE and low dark count probability at low excess bias is highly desirable for practical systems, because it relaxes the requirements for bias stability and temperature control, as well as improves the device reliability. This resultd agrees with theoretical analysis, which indicates that APDs with small k values have higher avalanche breakdown probability under a given normalized excess bias, V_e / V_{bd}.

Figure 23. Noise equivalent power versus discrimination level for InGaAs-on-Si SPAD at different DC biases.

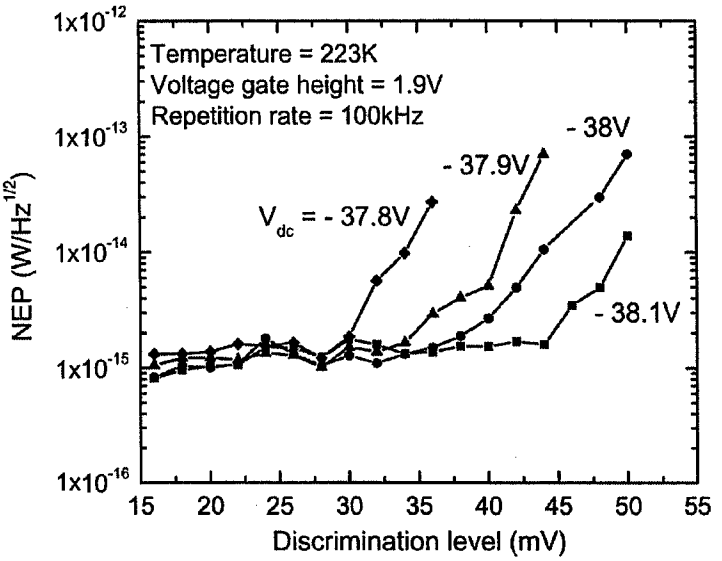

4. APD response to different numbers of input photons

Summary:

For the first time we obtained the response of Geiger-mode APDs for different numbers of photon or dark carriers. We have shown the avalanche probabilities for one, two, and three photons at different discrimination levels.

Detailed Discussion:

Although it has been shown that avalanche photodiodes (APDs) working in Geiger mode are able to detect single photons, there have been few studies on how Geiger-mode APDs respond to different numbers of input photons. The lack of such studies has been due partly to the notion that the APD output might be too noisy to render any useful information on photon number and partly to the unavailability of light sources able to generate specific photon numbers accurately. We have developed a method that can yield avalanche probabilities for Geiger-mode APDs under different numbers of photon excitation using the dark count measurement and a mathematical routine.

We assumed that the APD response to a dark carrier is equivalent to its response to a photo-carrier generated at the same time. Furthermore, since the dark count probability was typically much lower than 1%, we assumed that all the dark counts were caused by single carrier and therefore the APD response to dark carriers can represent its response to single photo-carrier. The APD is biased below its breakdown voltage and pulsed above breakdown for a few nanoseconds, under the so-called gated Geiger mode operation. The data presented here were obtained from a commercial InGaAs/InP APD that was biased below breakdown and pulsed above breakdown for 2 ns with various pulse voltages at a rate of 100kHz. The output avalanche coming out

of the APD was fed into a pulse counter. By measuring the count number at different discrimination voltage levels, V_{disc}, the output distribution of the Geiger-mode APD was obtained.

Figure 24 shows the measured dark count distribution at room temperature against the discrimination voltage. The dark count probability can be expressed as $P_d = 1 - \exp(-N_d P_{a1})$, where N_d is the number of dark carriers within the 2 ns pulse that may trigger avalanche events, and P_{a1} is the single-carrier initiated avalanche probability using V_{disc} as the measurement criteria. Since N_d is given by $I_{dm}\tau / q$, where I_{dm} and τ are the primary dark current and pulse width, one can directly calculate the "single-carrier induced avalanche probability" $P_{a1} = -q \ln(1 - P_d)/(I_{dm}\tau)$ as a function of V_{disc} from the data in Fig. 12. The probability density function (pdf) of a single-carrier initiated avalanche, dP_{a1}, is obtained by differentiating P_{a1} with respect to V_{disc}. One major step here is to derive the avalanche probability and pdf for 2-carriers, 3-carriers, (dP_{a2}, dP_{a3}) and so on as functions of V_{disc}. Because every carrier contributing to the output current must be the offspring of one of the carriers that initiate the avalanche, we can derive the following relation (Eq. 12).

$$dP_{an} = \int_0^V dP_{a1}(v) dP_{a(n-1)}(V - v)\, dv \Big/ \int_0^\infty \int_0^V dP_{a1}(v) dP_{a(n-1)}(V - v)\, dv\, dV \qquad (12)$$

From Eq. 12, we can further calculate dP_{an} dPan as long as we know all dP_{ai}'s where $i = 1, 2, \ldots, n-1$. Since we have obtained P_{a1} and dP_{a1} from the dark count measurement as stated before, we can hereby obtain Geiger-mode APD response to any number of input carriers. The avalanche probabilities density functions and avalanche probabilities caused by 1, 2, and 3 carriers are plotted against V_{disc} in Figures 13 and 14.

To our best knowledge, this is the first time that the relation between avalanche probability distribution and photon number is derived. For practical applications, this study shows us how to trade off APD sensitivity against dark count by setting the discrimination voltage. In the particular

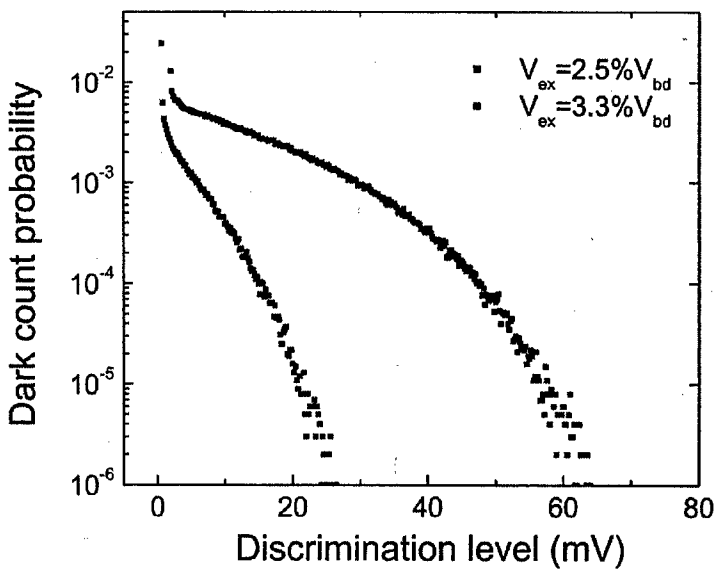

Figure 24. Measured dark count probability as a function of discrimination level at room temperature. V_{ex} is the excess pulse height on top of APD's breakdown and V_{bd} is the APD breakdown voltage.

case of Fig. 26, for example, one can set V_{disc} at 70 mV so the Geiger-mode APD has about 18% avalanche probability for 3 or more photocarriers but negligible dark counts since the probability of generating more than one dark carrier within the narrow time window even at room temperature is very low.

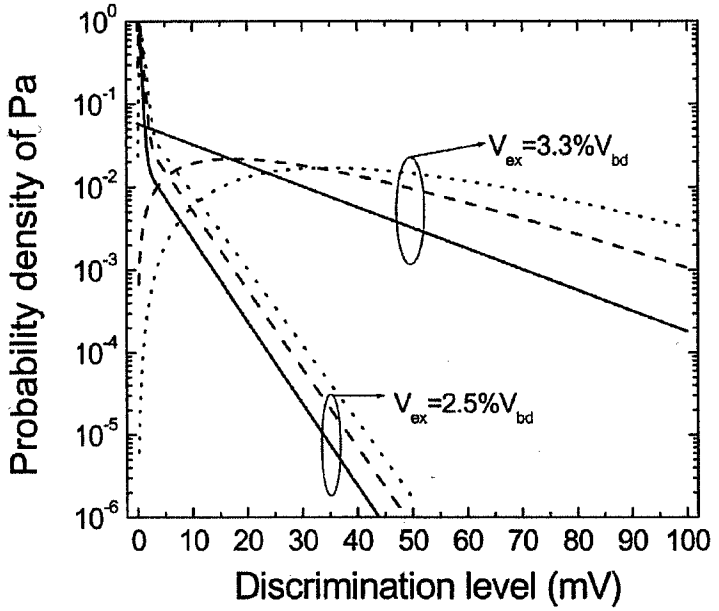

Figure 25. Probability density (dP_a) of one- (solid lines), two- (dash lines) and three-(dot lines) carrier initiated avalanche versus discrimination level, derived from the dark count measurement (Fig. 24) and Equation (12).

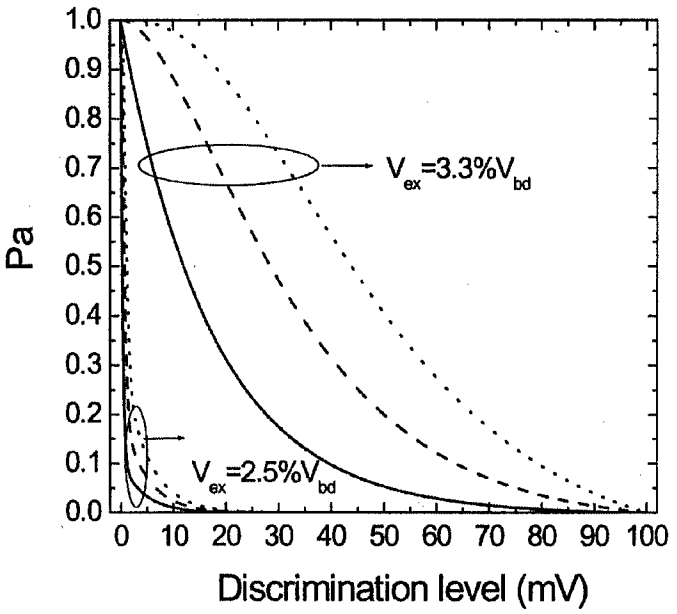

Figure 26. Dependence of avalanche probability on discrimination levels for one- (solid lines), two- (dash lines) and three (dot lines)-carrier initiated avalanche.

C. Optimization of low-noise InGaAs APDs for detection of single photons at telecom wavelengths (UT Austin)

In this reporting period we have focused on a study of the origin of dark counts in an $In_{0.53}Ga_{0.47}As$ / $In_{0.52}Al_{0.48}As$ SACM APD.

The type of photon-counting APD studied was a SACM (Separate-Absorption-Charge Multiplication) APD with a 1 μm-thick $In_{0.53}Ga_{0.47}As$ absorbing layer and 400nm-thick $In_{0.52}Al_{0.48}As$ multiplication layer. A schematic of the detector is shown in Figure 27. The structure was grown on n^+ substrate using metal-organic chemical vapor phase deposition (MOCVD). Top-illuminated mesa devices were fabricated using standard photolithography, lift off, wet chemical etching and SiO_2 passivation. Ti/Pt/Au and AuGe/Ni/Au were used as the p-contact and n-contact, respectively. Details of the structure and the processing can be found in Ref. [1].

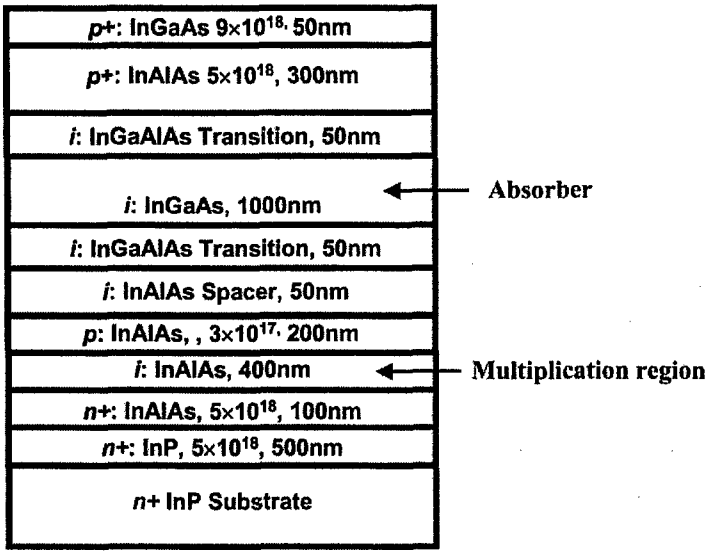

Figure 27. Schematic of $In_{0.53}Ga_{0.47}As$ / $In_{0.52}Al_{0.48}As$ APD

The device was investigated using the gated mode of operation. Figure 28 shows an Arrhenius plot of dark count rate at different excess voltages. These values of excess bias yield single photon detection efficiencies in the range ~10–15%. Since the dark counts exhibit an exponential dependence on temperature, an activation energy can be extracted from the slope of a plot of the logarithm of the dark count rate versus $1/kT$. The activation energies obtained from the plots range from 0.12 to 0.15eV for excess bias of 3.5V to 1.5V.

The value of activation energy can be used to identify the responsible mechanism. The following mechanisms are possible thermal sources of dark counts in the SACM APD:

1) Dark counts resulting from diffusion of carriers from quasi-neutral n- and p-regions to the multiplication layer have an exponential dependence on temperature through the band gap. Hence the activation energy is expected to be

equal to the band gap of the neutral region.

2) For dark counts resulting from generation-recombination in the $In_{0.53}Ga_{0.47}As$ absorber layer, the activation energy is expected to be ~ ½ the band gap of $In_{0.53}Ga_{0.47}As$, which is ~ 0.35eV.
3) For generation-recombination in the multiplication layer, the activation energy should be ~ ½ band gap of $In_{0.52}Al_{0.48}As$, which is 0.67eV.

The experimentally-observed activation energy is much lower than the value expected from any of the mechanisms mentioned above. In the following, we explain the temperature dependence of dark count rate by invoking band-to-band tunneling in the multiplication layer. Band profile simulations of the device above breakdown voltage indicate a triangular barrier for tunneling.

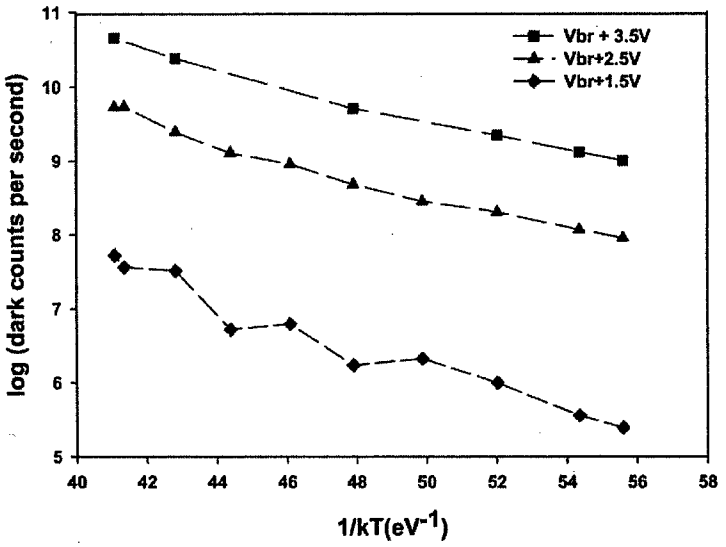

Figure 28. Dark count rate as a function of 1/kT for different excess voltages.

Dark counts due to tunneling ($N_{d,tunneling}$) can be estimated by dividing the tunneling dark current, $I_{tunneling}$, by the electronic charge, q, and multiplying by the breakdown probability, $P_{eh}(junction)$.

$$N_{d,tunneling} = P_{eh}(junction) \cdot C_1 \cdot V_a \cdot i \qquad (1)$$

$P_{eh}(junction)$ is the electron-hole pair breakdown initiation probability at the junction, where the electric field is maximum[2]. A more thorough analysis involves integrating the product of the generation rate due to band-to-band tunneling and position-dependent breakdown probability over the depletion layer width.

The dark counts per second due to tunneling can be written as [3]:

$$N_{d,tunneling} = P_{eh}(junction) \cdot C_1 \cdot V_a \cdot E_m \cdot \exp\left(\frac{-C_2}{E_m}\right). \quad (2)$$

C_1 can be expressed as

$$C_1 = \sqrt{\frac{2 \cdot m_r^*}{E_g}} \cdot \frac{q^2}{4 \cdot \pi^3 \cdot \hbar^2} \quad (3)$$

The form of C_2 depends on the type of tunneling barrier. For a triangular barrier,

$$C_2 = \exp\left(-\frac{4 \cdot \sqrt{2 \cdot m_r^*} \cdot E_g^{3/2}}{3 \cdot q \cdot \hbar \cdot E_m}\right) \quad (4)$$

The various terms in equations (2)-(4) are described below. E_m is the electric field in the multiplication region. Equation (2) is derived assuming a constant electric field in the depletion layer [4]. Since the electric field in the multiplication layer of an SACM APD is not constant, the average electric field, obtained by solving Poisson's equation for the SACM APD with appropriate boundary conditions, was used in the calculation. V_a is the voltage drop across the junction, E_g is the band gap of $In_{0.52}Al_{0.48}As$, $\hbar$ is Planck's constant, and m_r^* is the tunneling effective mass. Its value is taken to be the reduced effective mass defined as follows,

$$\frac{1}{m_r^*} = \frac{1}{m_e^*} + \frac{1}{m_{lh}^*}, \quad (5)$$

where, $m_e^* = 0.079\, m_o$ is the Γ valley electron effective mass and $m_{lh}^* = 0.086\, m_o$ is the light hole effective mass for $In_{0.52}Al_{0.48}As$. Note that equation (2) applies only to direct tunneling, which is dominant for direct band gap $In_{0.52}Al_{0.48}As$.

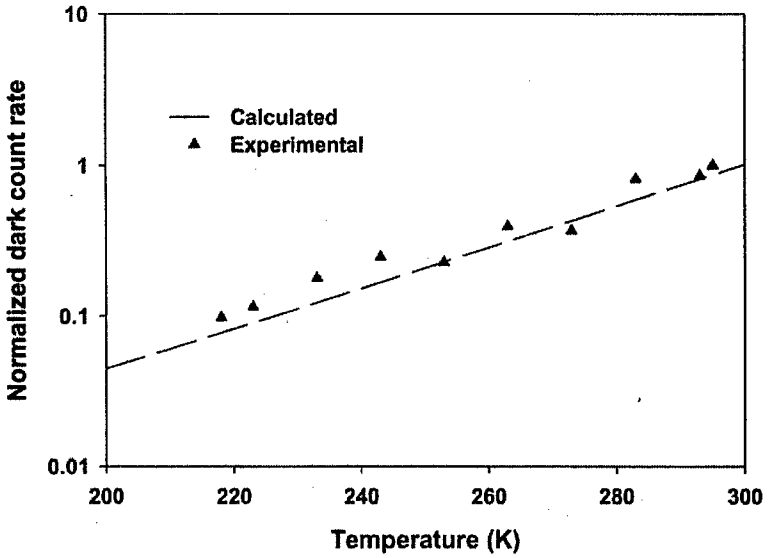

Figure 28. Experimental and calculated dark count rate as a function of temperature for excess bias of 1.5V.

Figure 28 shows the calculated dark count rate as a function of temperature, normalized to the value at room temperature. It should be noted that the absolute value of dark count rate depends on experimental details: for example, the discriminator threshold, the quenching technique, and the repetition rate. Also, the simple tunneling model does not take into account non-uniformities in the active area. However, regardless of the absolute value of the dark counts, for a given excess voltage their temperature dependence is unique. The temperature dependence of dark count rate is primarily due to the temperature dependence of the band gap of $In_{0.52}Al_{0.48}As$. Figure 29 shows a plot of the $E_g^{3/2}$ of $In_{0.52}Al_{0.48}As$ versus $1/kT$, using the temperature dependence of the band gaps of InAs and AlAs and the bowing parameter for $In_{0.52}Al_{0.48}As$. In the temperature range of 200K to 300K, $E_g^{3/2}$ has an almost linear dependence on $1/kT$ with the slope $\alpha = 4.8\times10^{-3}\ eV^{5/2}$. Using $E_g^{3/2}$ as a linear function of $1/kT$, a plot of the log of dark count rate versus $1/kT$ has a slope of $\left(-\frac{4\cdot\sqrt{2\cdot m_r^*}\cdot\alpha}{3\cdot q\cdot\hbar\cdot E_m}\right)$.
The activation energy expected from this expression at an excess bias of 3.5V is 0.14eV, which matches reasonably well with the experimentally observed value of 0.11eV. The activation energy depends inversely on electric field in the multiplication layer, which was also observed experimentally.

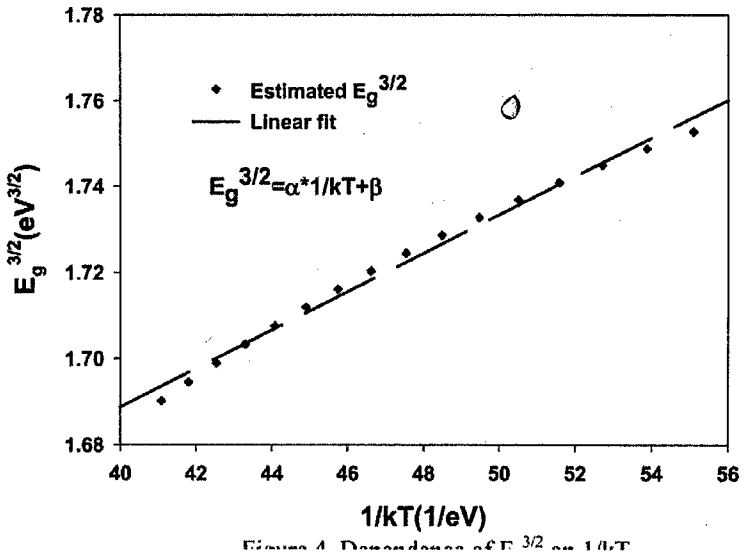

Figure 29. Dependence of $E_g^{3/2}$ on 1/kT.

It is interesting to note that in this device, even though the dark count generation mechanism is dominated by tunneling, it is not the primary dark current generation mechanism below breakdown. Figure 30 shows the dark current below breakdown voltage for the device at various temperatures. For a broad range of voltages above the punch through value, the activation energy is 0.4 eV. This points to generation-recombination in $In_{0.53}Ga_{0.47}As$ as the responsible mechanism.

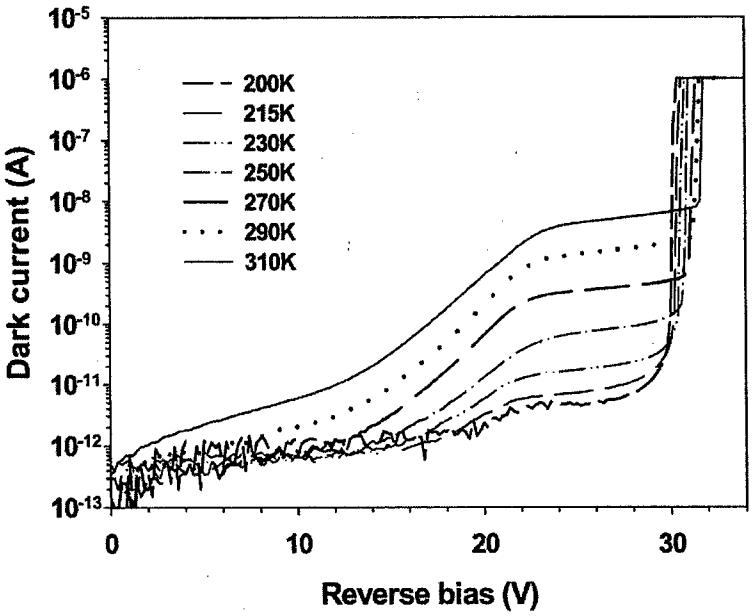

Figure 30. Dark current as a function temperature

The dominance of band-to-band tunneling in Geiger mode operation for this device is attributed to high electric field in its thin multiplication layer of 400 nm. However such thin multiplication layer results in very good timing performance. A 75-μm diameter device exhibits timing jitter of only 60 ps at 200 K when operated at 3.5V above breakdown voltage. Thus there is a trade off between the timing performance of a Geiger mode APD and tunneling in its multiplication layer. Since tunneling current is very sensitive to electric field, we estimate that increasing the multiplication layer thickness by a factor of 2 will reduce the tunneling induced dark counts by 3 orders of magnitude. The increased thickness of the multiplication layer is also expected to give a steeper increase in breakdown probability with excess voltage, and hence improved single photon counting performance [5]. Ultimately generation-recombination in the multiplication layer and avalanche build up time will determine the optimum multiplication layer thickness.

In summary, the origin of dark counts in an $In_{0.53}Ga_{0.47}As$ / $In_{0.52}Al_{0.48}As$ SACM APD was studied using the temperature dependence of the dark count rate. The dark count rate in these APDs was found to be dominated by band-to-band tunneling in the multiplication layer.

D. Detection of Single Photons Using Sum -Frequency Generation

Another approach to detection of single photons at telecom wavelengths that has been pursued under this program is to use sum-frequency generation to increase the energy of the single photon so that a silicon APD can be used for detection. The proposed implementation uses a periodically-poled lithium niobate (PPLN) waveguide to produce efficient sum-frequency mixing of a strong C-band pump (~1510 nm) and a weak C-band signal

[2] W. J. Kindt, "Geiger mode ava-

(~1550 nm) to produce a signal at the sum frequency (~710 nm), which can be detected using a Geiger-mode silicon APD. Overall, the effort devoted to this approach has been less than originally planned, because as the QuIST program evolved, we believed that pursuing

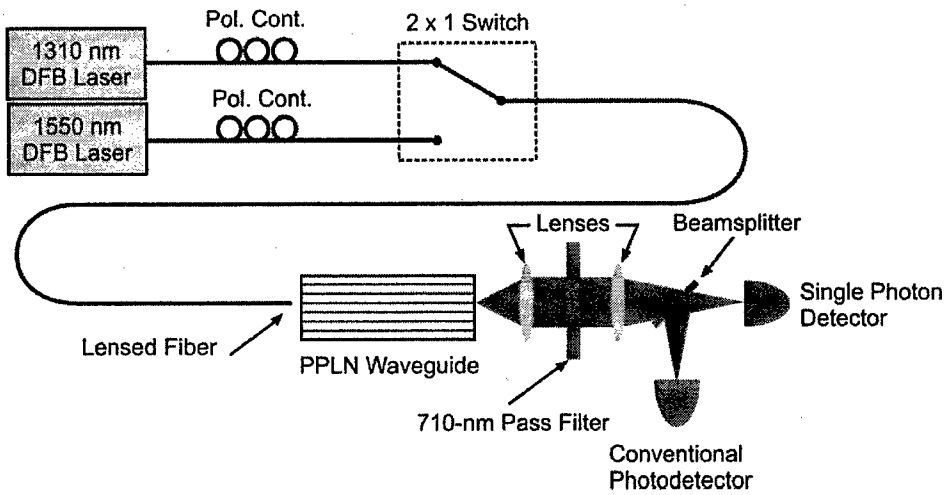

Figure 31. Experimental set-up for testing the sum-frequency generation approach to single photon detection.

the integrated detector electronics described above represented a more immediate contribution to this program and to the field of quantum key distribution. However, in earlier years we made some preliminary measurements (such as the sensitivity of silicon detectors at telecom wavelengths). In Year Three of the program, we assembled and tested a preliminary set-up for investigating sum-frequency generation (Figure 31).

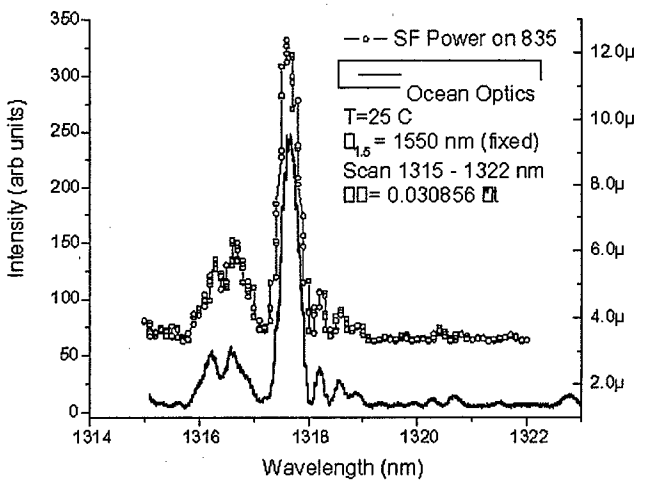

Figure 32. Scans of sum-frequency output versus O-band wavelength.

The arrangement shown in Figure 31 allowed light in both the O-band and C-band wavelength ranges to be coupled simultaneously into the PPLN waveguide. A fiber with a lensed end was used for efficient coupling into the waveguide, which was mounted on a temperature-controlled stage. Both the temperature of the PPLN crystal and the wavelength of the input light could be tuned in order to achieve phasematching.

Figure 32 shows the variation of the intensity at the sum-frequency as the wavelength of

the O-band input is scanned while the wavelength of the C-band input is held constant at 1550 nm. Phasematching for sum-frequency generation occurs when the shorter-wavelength is tuned to 1317.6 nm, producing light at a sum-frequency of 712 nm.

Preliminary characterization of these waveguides revealed several unanticipated aspects of their behavior. Although a sum-frequency signal was detected, self-doubling of the O-

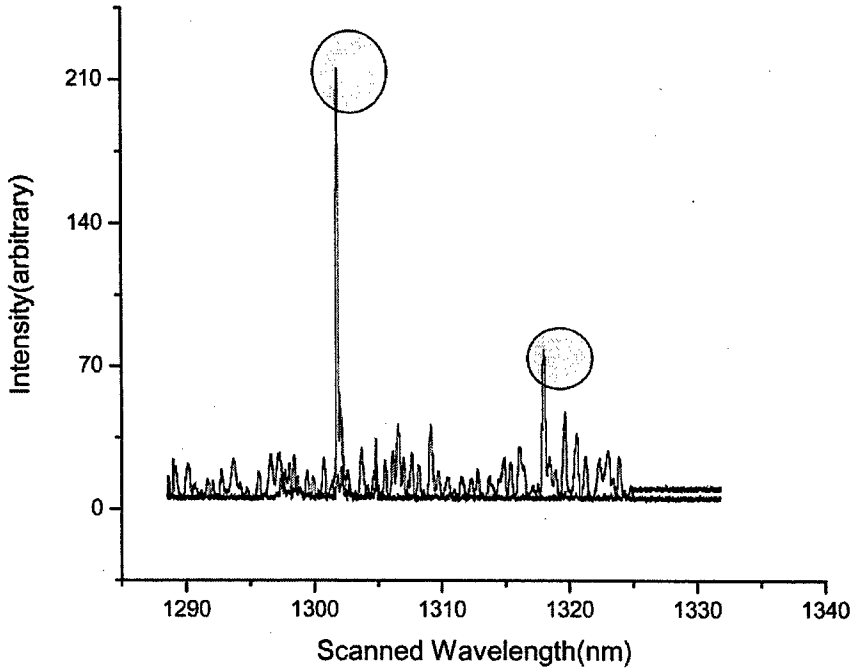

band signal was considerably stronger. This behavior was unexpected, given the design of the PPLN waveguide, which should not provide phasematching for a strong self-doubling interaction. We are continuing to investigate the cause of this behavior.

III. Year Three Publications

1. Bethune, DS; Risk, WP; Pabst, GW. 2004. A high-performance integrated single-photon detector for telecom wavelengths. JOURNAL OF MODERN OPTICS 51 (9–10): 1359–1368.
2. Karve, G.; Li X.; Wang S.; Ma F.; Campbell J.C., Ispasoiu R., J.C.; Kinsey G.S.; Boisvert J.C.; Isshiki, T.D.; Sudharsanan R.; Bethune D.S.; Risk W.P., "Study of dark counts in Geiger mode $In_{0.53}Ga_{0.47}As$ / $In_{0.52}Al_{0.48}As$ SACM APDs", Proceedings of IEEE LEOS Annual Conference, (2004).
3. Karve, G.; Li X.; Wang S.; Ma F.; Campbell J.C., Ispasoiu R., J.C.; Kinsey G.S.; Boisvert J.C.; Isshik, T.D.; Sudharsanan R.; Bethune D.S.; Risk W. P., "Origin of dark counts in $In_{0.53}Ga_{0.47}As$ / $In_{0.52}Al_{0.48}As$ avalanche photodiodes operated in Geiger mode", submitted to Applied Physics Letters.

IV. References

1. C. Hu, K.A. Anselm, B.G. Streetman, and J.C. Campbell, "Noise characteristics of thin multiplication region GaAs avalanche photodiodes," *Appl. Phys. Lett.*, 69, pp. 3734–3736 (1996).

2. C. Lenox, P. Yuan, H. Nie, O. Baklenov, C. Hansing, J. C. Campbell, and B. G. Streetman, "Thin Multiplication Region InAlAs Homojunction Avalanche Photodiodes," *Appl. Phys. Lett.*, 73, pp. 783–784 (1998).

3. P. Yuan, K. A. Anselm, C. Hu, H. Nie, C. Lenox, B. G. Streetman, and J. C. Campbell, "A New Look at Impact Ionization - Part II: Gain and Noise in Short Avalanche Photodiodes," *IEEE Trans. Electron Dev.*, 46, pp. 1632–1639 (1999).

4. P. Yuan, C. C. Hansing, K. A. Anselm, C. V. Lenox, H. Nie, A. L. Holmes, Jr., B. G. Streetman, and J. C. Campbell, "Impact Ionization Characteristics of III-V Semiconductors for a Wide Range of Multiplication Region Thicknesses," *IEEE J. Quantum Electron.*, 36, 198–204 (2000).

5. R. J. McIntyre, "A New Look at Impact Ionization - Part I: A Theory of Gain, Noise, Breakdown Probability, and Frequency Response," *IEEE Trans. Electron. Dev.*, 46, pp. 1623–1631 (1999).

6. A. R. Hawkins, W. Wu, P. Abraham, K. Streubel, and J. E. Bowers,"High Gain-Bandwidth-Product Silicon Heterointerface Photodetector," *Appl. Phys. Lett.*, 70, pp. 303–305 (1997).

7. D. S. Bethune and W. P. Risk, "An Autocompensating Fiber-Optic Quantum Cryptography System Based on Polarization Splitting of Light," *IEEE J. Quantum Electron.*, 36(3), 340 (2000).

8. Donald S. Bethune, Martha Navarro, William P. Risk, "Enhanced Autocompensating Quantum Cryptography System," *Appl. Opt.-LP*, 41, 1640 (2002).

9. Fujitsu Compound Semiconductor, Inc., 2355 Zanker Rd., San Jose, Calif. 95131 (http://www.fcsi.fujitsu.com).

10. Id Quantique SA; Rue Cingria, 10; 1205 Genève, Switzerland (http://www.idquantique.com).

11. Akihisa Tomita, "High Performance Photon Detector for Qubit Discrimination in 1550 nm," *NEC Res. & Dev.*, 44 (3) 290-293 (2003).

12. H. Kosaka, A. Tomita, Y. Nambu, T. Kimura and K. Nakamura, "Single-photon interference experiment over 100 km for quantum cryptography system using a balanced gated-mode photon detector," http://xxx.lanl.gov/abs/quant-ph/0306066 (June 2003).

13. Akihisa Tomita and Kazuo Nakamura, "Balanced, gated-mode photon detector for quantum-bit discrimination at 1550 nm," *Opt. Lett.*, 27, 1827-1829 (2002).

14 D. Stucki, N. Gisin, O. Guinnard, G. Ribordy and H. Zbinden, "Quantum key distribution over 67 km with a plug&play system," *New J. Physics*, 4, 41.1-41.8 (2002).

15. A. Yoshizawa, R. Kaji and H. Tsuchida, "After-pulse-discarding in single-photon detection to reduce bit errors in quantum key distribution," *Optics Express*, 11, 1303-1309 (2003).

G. Karve, X.-G. Zheng, X.-F. Zhang, X. Li, N. Li, S. Wang, F. Ma, A. L. Holmes, Jr., J. C. Campbell, G. S. Kinsey, J. C. Boisvert, T. D. Isshiki, R. Sudharsanan, D. S. Bethune, W. P. Risk, IEEE J. Quantum Electronic **39**, 1281 (2003).

[2] W. J. Kindt, "Geiger mode avalanche photodiode arrays for spatially resolved single photon counting", (Delft University press, 1999).

[3] R. H. Haitz, **36**, 3123 (1965).

[14] E.O.Kane, J. Appl. Phys. **32**, 83 (1961).

[5] Shuling Wang, Feng Ma, Xiaowei Li, Karve, G., Xiaoguang Zheng, and J. C. Campbell, Appl. Phys. Lett. **82**, 1971 (2003).